Measurement of conversion electrons with the ^{208}Pb(p, n)^{208}Bi reaction and derivation of the shell model proton neutron hole interaction from the properties of ^{208}Bi

K. H. Maier,[1,2,3] T. Kibédi,[2] G. D. Dracoulis,[2] P. Boutachkov,[4] A. Aprahamian,[4] A. P. Byrne,[2,5] P. M. Davidson,[2] G. J. Lane,[2] M. Marie-Jeanne,[6,7] P. Nieminen,[2] and H. Watanabe[2]

[1]*Niewodniczański Institute of Nuclear Physics, PAN, Kraków, Poland*
[2]*Department of Nuclear Physics, Research School of Physical Sciences and Engineering,*
Australian National University, Canberra ACT 0200, Australia
[3]*SUPA, School of Engineering and Science, University of Paisley, Paisley PA1 2BE, United Kingdom*
[4]*Physics Department, University of Notre Dame, Notre Dame, Indiana 46556, USA*
[5]*Department of Physics, The Faculties, Australian National University, Canberra ACT 0200, Australia*
[6]*Ecole Nationale Supérieure d'Ingenieurs de Caen, F-14050 Caen Cedex, France*
[7]*CERN, PH-IS Division, CH-1211 Geneva 23, Switzerland*
(Received 31 July 2007; published 5 December 2007)

Conversion electrons from ^{208}Bi have been measured using singles and coincidence techniques with the ^{208}Pb(p, n)^{208}Bi reaction at 9 MeV. The new information on multipolarities and spins complements that available from recent γ-γ-coincidence studies with the same reaction [Boutachkov *et al.*, Nucl. Phys. A768, 22 (2006)]. The results on electromagnetic decays taken together with information on spectroscopic factors from earlier single-particle transfer reaction measurements represent an extensive data set on the properties of the one-proton one-neutron-hole states below 3 MeV, a spectrum which is virtually complete. Comparison of the experimental observables, namely, energies, spectroscopic factors, and γ-branching ratios, with those calculated within the shell model allows extraction of the matrix elements of the shell model residual interaction. More than 100 diagonal and nondiagonal elements can be determined in this way, through a least squares fit to the experimental data. This adjustment of the interaction significantly affects the calculated properties of the γ-ray transitions. Nevertheless, the matrix elements thus obtained are remarkably similar to those of a realistic interaction calculated from free-nucleon scattering. Characteristic features of the interaction are discussed.

I. INTRODUCTION

Understanding the interaction between the nucleons inside the nucleus is a central theme of nuclear physics. In the shell model, this translates to characterization of the single-particle energies and the residual two-body interaction between the particles, whereas three-body and higher contributions are usually neglected. Most single-particle energies close to stable doubly magic nuclei are known from experiment, but relatively few matrix elements of the two-body residual interaction have been determined experimentally. This is particularly so for the nondiagonal elements. The coarse features of the interaction are well known and can be reproduced, even by schematic forces like the surface delta interaction (SDI). However, since the pioneering work of Kuo and Brown [2], the residual interaction inside the nucleus can also be calculated from that between free nucleons as measured by scattering. These calculations have made substantial progress recently through the use of a low momentum interaction [3]. Also, more advanced calculations have been performed for the neutrons above ^{132}Sn, which occupy the same orbitals as treated here [4].

The initial aim of the present work was to obtain new experimental information on the excited states of ^{208}Bi, principally through conversion electron measurements. This was followed by a determination of the elements of the residual interaction by a fit of the calculated properties to all the available experimental data. Many elements of the interaction between proton particles and neutron holes,

particularly nondiagonal ones, were determined in this way. The analysis included sets of matrix elements for all spins, involving many combinations of configurations.

The ^{208}Bi nucleus consists of a proton particle and a neutron hole relative to the doubly magic ^{208}Pb, allowing a direct determination of the shell model residual interaction between these valence particles from the observed levels and their properties. The level scheme and γ transitions in ^{208}Bi have been recently studied by Boutachkov *et al.* [1] using the ^{208}Pb(p, n)^{208}Bi reaction. We report here on the measurement of conversion electrons with the same reaction. The results include the determination of new multipolarities and mixing ratios and also confirm the conclusions on spins and multipolarities from the γ-ray measurements [1]. The statistical nature of the compound nuclear reaction should lead to the population of all levels of low and medium spin and therefore give a practically complete level scheme. In contrast, transfer reactions, including ^{207}Pb(^{3}He,d)^{208}Bi [5] and ^{209}Bi(p, d)^{208}Bi [6], selectively populate states with specific particle-hole configurations [7]. Taken together, these reactions give relatively complete, detailed, and reliable knowledge of the proton-particle neutron-hole states relative to ^{208}Pb.

The results on level energies, spectroscopic factors, and γ-branching ratios are examined in the second part of this article in the context of the associated properties predicted by the shell model with selected residual interactions. With a

realistic interaction obtained from free-nucleon scattering as a starting point, the interaction matrix elements are determined by optimizing the agreement between calculated and measured values through a nonlinear least-squares fit. Of a total of about 1000 matrix elements, approximately 150 significantly affect the experimental observables. The empirical interaction so determined should allow more meaningful calculations of the properties of neighboring nuclei and give hints of improvements of the calculations of the interaction.

II. ELECTRON MEASUREMENTS AND RESULTS

Conversion electrons were measured using a superconducting solenoidal spectrometer [8,9] to transport electrons to cooled Si(Li) detectors in several configurations, as described below. A beam of 9 MeV protons provided by the Australian National University 14UD Pelletron accelerator struck a metallic Pb target enriched to 98.5% in ^{208}Pb and was stopped in a Faraday cup 1 m behind the target. The target was tilted so that its surface was at $30°$ degrees to the beam direction, to minimize the effect of straggling on electrons emerging from the rear of the target. The beam energy was chosen to match the conditions of the previous γ-ray measurement [1]. Simultaneously with the electron measurements, single γ rays were measured with a Compton-suppressed Ge detector at $135°$ to the beam axis and 25 cm distance from the target [9]. The two electron measurements, with the above common features, will be further described in the following sections.

A. Electron-electron coincidence measurements

For the electron-electron coincidence measurements, a cooled Si(Li) detector array [10] was mounted on the long side of the spectrometer at 43 cm from the target. This array consists of six independent triangular detectors, each 4.3 mm thick, which are arranged in a hexagon of 66 mm outer diameter. There is an inner dead zone of 11 mm in diameter. Electron-electron coincidences can be measured by requiring coincidences between any pair of detectors. The solenoid field was adjusted to guide electrons below 1200 keV onto the detectors. To suppress low energy atomic electrons reaching the detectors, rather than using mechanical obstructions, a hollow cylindrical electrode, charged to -20 kV potential, was inserted between the target and detector [11]. The resolution was 2.5 keV full width at half maximum for the 291.6 keV K line.

An additional magnetic-field-immune Ge detector was inserted into the spectrometer from the short side to measure electron-γ coincidences simultaneously. The front face of this detector was about 3 cm from the target. To optimize the energy resolution of the electron array for the coincidence measurements involving low energy conversion electrons, a thin 0.8 mg/cm^2 target was used. The measuring time with a 0.4 nA beam was 40 h. Data were taken in event-by-event mode, the measured parameters being the energies from each element of the electron array and the Ge (coincidence) detector, and their time relative to a common reference pulse train. From these measured times, the relative time between any two detectors was evaluated. The single γ spectrum was also recorded using the Compton-suppressed Ge detector.

The data were sorted into $E_e \times E_e$ and $E_e \times E_\gamma$ matrices of 4k × 4k channels. Both a prompt time window of ± 140 ns around the prompt peak and appropriate random background windows were taken to produce these matrices corrected for random events for subsequent analysis.

B. Lens mode single-electron measurements

In the second set of measurements, the spectrometer was operated in the lens mode to measure singles electrons, as described in Ref. [9]. A beam of $\sim$30 nA of 9 MeV protons was incident on a 3.3 mg/cm^2 target. The measuring time was 36 h, and the beam was chopped with periods of 0.5 ms on and 0.5 ms off. The target was also viewed by a Compton suppressed Ge detector.

The electrons were measured by a 10 mm thick and 20 mm diameter, cooled Si(Li) detector. At a fixed field, the lens accepts an electron momentum interval with a width of 12% [9]. The field was swept to accept electrons from 80 to 2200 keV in the center of the acceptance interval, with the stepping of the field controlled by the integrated current in the Faraday cup. The energy dependence of the electron efficiency was calculated from the known, momentum-dependent transmission through the lens [9], taking into account the energy and angular dependence of the response function of the Si(Li) detector for electrons. These calculations agreed with measurements of a ^{152}Eu radioactive source. The resolution was 4 keV for the 601 keV K line.

Data were measured in event-by-event mode. Each event contained, in addition to the electron or γ-ray energy, the time relative to the beam chopping, and the instantaneous magnetic field. The time information was used to isolate and remove electrons and γ rays arising from long-lived background radiation, while the magnetic field information was used to perform momentum matching [9], allowing rejection of events in the electron detector that arose from backscattering, for example. There was little long-lived background.

C. Evaluation of conversion coefficients

The bottom panel of Fig. 1 shows the electron spectrum measured in lens mode in the present work, while the top panel presents the spectrum of single γ rays of Ref. [1]. This γ-ray spectrum, recorded with a detector close to a thick target, was used to deduce the conversion coefficients, since the γ-ray spectrum of the present measurements showed some impurity peaks, mainly due to neutrons produced by the beam after passing the target. No significant differences due to the differences in target thickness have been found for the relative intensities of the clean lines between the two γ measurements. The measurements of Ref. [1] had also shown that the nuclei are not significantly aligned, and the angular distributions of the γ rays are correspondingly isotropic. Therefore the conversion coefficients can be evaluated without uncertainties due to angular dependence of the intensities. As two different measurements were used, electron and γ-ray intensities had to be normalized to each other. This was done at the clean K conversion line ($\alpha_K = 0.544$) of the 263 keV transition (see Fig. 1).
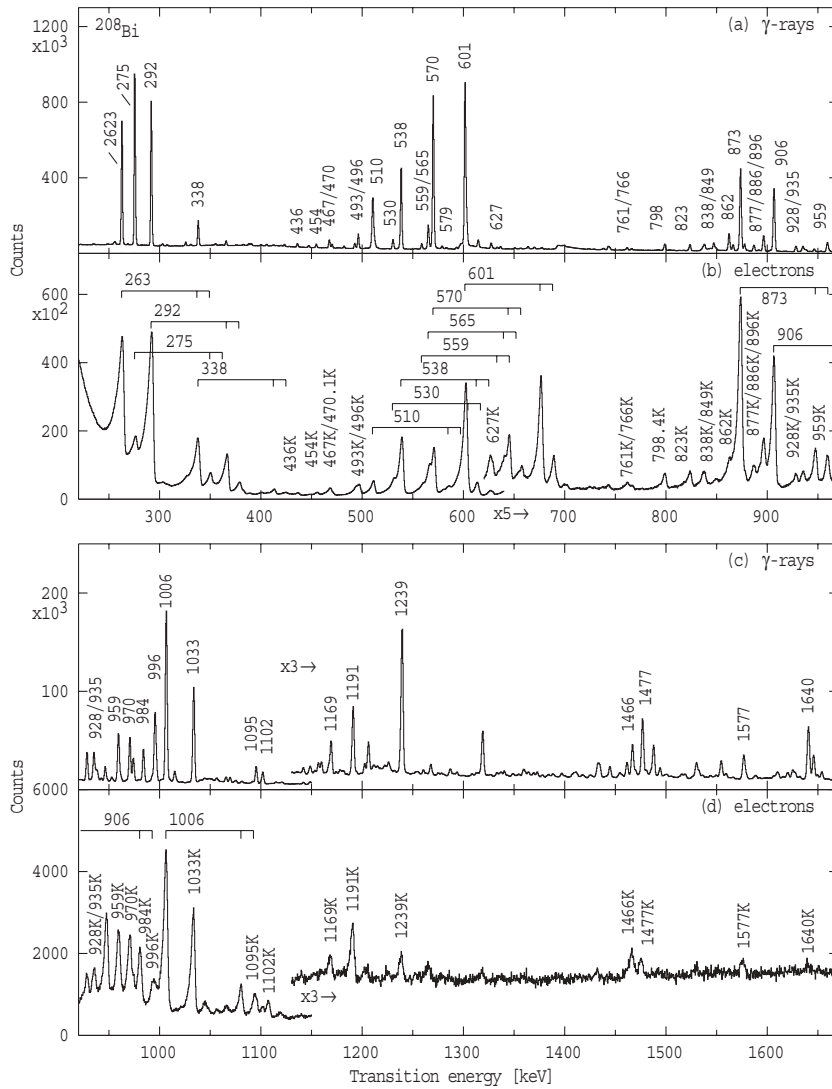
FIG. 1. Single γ (a) and (c) from Ref. [1] and conversion electron (b) and (d) spectra for transitions in ^{208}Bi. The electron spectrum is adjusted so that the K conversion lines are aligned with the corresponding γ-ray transition energies.

The electron spectrum is complicated, containing many overlapping peaks; and for some lines, unambiguous determination of the background level is difficult. Systematic errors depending on the choice of fit parameters, such as background levels and number of peaks, turn out to be more important than statistics. Therefore the electron spectra were fitted a number of times with different choices of parameters, and the difference of the intensities obtained were taken as one indication of the experimental uncertainties. It is not possible to determine the uncertainties unambiguously, although the situation is constrained since the γ measurements of Ref. [1] indicate which lines would be present in the electron spectrum and therefore where problems from overlapping lines could occur. The measured K conversion coefficients are shown in Fig. 2 and compared with theoretical values calculated with the program BRICC [12]. These values are partly for known transition multiplets, which can only be separated in the γ-γ coincidence spectra [1]. For example, the 275 keV transition is a doublet of a strong $E1$ and a weak $M1$ transition. Nearly all coefficients are compatible with dominant or pure $M1$ transitions.

Figure 3 shows a fit to the total projection of the electron-electron coincidence measurement. For a given multipolarity, the energy separation and intensity ratios for the various subshell conversion electron lines have been fixed to those expected from the theoretical conversion coefficients and from multipolarities deduced from the lens measurements. While the 263 and 291 keV transitions are pure $M1$ transitions, the 275 keV transition was assumed to be a doublet of a 93% $E1$ component and a 7% $M1$ component, as determined in the previous γ-ray measurement [1]. From the electron spectrum, since the conversion line is stronger, the energy of the $M1$ component can be better determined [275.6(2) keV] than that from the γ-ray measurements, which gave 275.3(2) keV. Note that the line shape for the L and M (composite) lines is sensitive to the subshell ratios, hence the extracted L or M intensities depend strongly on the assumed multipolarity. For a 263 keV transition, the K/L ratio for $E2$ is four times smaller than for $M1$, and therefore even small $E2$ admixtures in the $M1$ transitions would be clearly visible.

Table I gives the K and L shell conversion coefficients measured in lens mode. Multipolarities have

TABLE I. Experimental conversion coefficients and transitions in ^{208}Bi. Transition energies E_γ and for multiplets fraction of γ intensity I_γ (in %) from the data of Ref. [1]. The 1st and the 2nd multipoles and their fractions are deduced from the experimental conversion coefficient α_{exp}. The main multipole is given in boldface. Electron and γ intensities have been normalized at the 262.5 keV line. A 10% uncertainty of this normalization is not included in the quoted experimental conversion coefficient values.

E_γ (keV)	I_γ (%)	E_{ini} (keV)	Transition	Shell	α_{exp}	Mult. 1 (%)	Mult. 2 (%)
262.5		1802.2	$1^+ \to 2^+$	K	$\equiv 0.544$	$\equiv$ **M1**	
275.3	93 (3)	2077.6	$2^- \to 1^+$	K	0.064(8)	$M1$ 7 (2)	**E1** 93 (2)
275.3	7 (3)	2478.4	$\to ?^-$	L	0.019(7)	$M1$ 17 (9)	**E1** 83 (9)
291.6		924.8	$2^+ \to 3^+$	K	0.47(3)	**M1**	
337.9		2415.7	$? \to 2^-$	K	0.36(10)	**M1**	$E2 \leqslant 10$
				L	0.056(11)	**M1**	$E2 \leqslant 10$
435.7	30 (20)	1069.1	$3^+ \to 3^+$	K	0.14(4)	**M1**	$E2 \leqslant 40$
435.9	70 (20)	1469.4	$5^+ \to 4^+$				
454.4		2657.3	$\to ?^-$	K	0.11(4)	**M1**	$E2 \leqslant 50$
467.4	70 (20)	1069.1	$3^+ \to 4^+$	K	0.083(20)	**M1**	$E2 \leqslant 60$
467.2	30 (20)	2544.8	$\to 2^-$				
470.1		1539.4	$2^+ \to 3^+$	K	0.12(7)	**M1**	$E2 \leqslant 60$
492.5		2570.2	$\to 2^-$	K	0.102(27)	**M1**	$E2 \leqslant 30$
$495.9 \geqslant 90$		1529.4	$3^+ \to 4^+$	K	0.085(14)	**M1**	
510.2		510.2	$6^+ \to 5^+$	K	0.065(15)	**M1**	$E2 \leqslant 60$
$529.9 \geqslant 50$		1563.5	$4^+ \to 4^+$	K	0.088(11)	**M1**	$E2 \leqslant 10$
538.2		601.4	$4^+ \to 4^+$	K	0.075(6)	**M1**	$E2 \leqslant 20$
				L	0.0110(25)	**M1**	$E2 \leqslant 60$
558.5		2478.4	$\to 3^-$	K	0.058(15)	**M1**	$E2 \leqslant 50$
565.1		628.3	$5^+ \to 4^+$	K	0.056(7)	**M1**	$E2 \leqslant 40$
				L	0.0110(26)	**M1**	$E2 \leqslant 50$
569.9		633.1	$3^+ \to 4^+$	K	0.0312(22)	$M1$ 29 (4)	**E2** 71 (4)
				L	0.0060(6)	$M1$ 19 (8)	**E2** 81 (8)
601.4		601.4	$4^+ \to 5^+$	K	0.065(7)	**M1**	$E2 \leqslant 1$
				L	0.0114(12)	**M1**	
627.1		1563.5	$4^+ \to 3^+$	K	0.059(13)	**M1**	$E2 \leqslant 50$
				L	0.007(4)	**M1**	$E2 \leqslant 100$
761.3		2838.9	$\to 2^-$	K	0.035(12)	**M1**	$E2 \leqslant 40$
765.7		2843.3	$\to 2^-$	K	0.028(11)	**M1**	$E2 \leqslant 70$
798.4		2718.5	$\to 3^-$	K	0.029(6)	**M1**	$E2 \leqslant 30$
823.2		886.4	$5^+ \to 4^+$	K	0.030(7)	**M1**	$E2 \leqslant 10$
837.7		1870.7	$3^+ \to 4^+$	K	0.026(6)	**M1**	$E2 \leqslant 30$
849.0		1882.1	$4^+ \to 4^+$	K	0.025(7)	**M1**	$E2 \leqslant 40$
861.8		924.8	$2^+ \to 4^+$	K	0.0060(20)	$M1 \leqslant 10$	**E2**
873.3		936.2	$3^+ \to 4^+$	K	0.0205(18)	**M1**	$E2 \leqslant 20$
877.2		1802.2	$1^+ \to 2^+$	K	0.014(3)	$M1 \leqslant 70$	**E2**
$886.4 \geqslant 80$		886.4	$5^+ \to 5^+$	K	0.023(4)	**M1**	
896.0	80	959.0	$4^+ \to 4^+$	K	0.0195(25)	**M1**	$E2 \leqslant 30$
896.2	20	1529.4	$3^+ \to 3^+$				
906.3		1539.4	$2^+ \to 3^+$	K	0.0183(25)	**M1**	$E2 \leqslant 30$
				L	0.0030(5)	**M1**	$E2 \leqslant 50$
$928.0 \geqslant 90$		1529.4	$3^+ \to 4^+$	K	0.0140(23)	**M1**	
934.7	60 (25)	1870.7	$3^+ \to 3^+$	K	0.015(5)	**M1**	$E2 \leqslant 70$
935.2	40 (25)	1563.5	$4^+ \to 5^+$				
959.0	50 (30)	959.0	$4^+ \to 5^+$	K	0.0216(18)	**M1**	
959.0	50 (30)	1469.4	$5^+ \to 6^+$				
970.2		1033.2	$4^+ \to 4^+$	K	0.015(3)	**M1**	$E2 \leqslant 50$

TABLE I. (*Continued.*)

E_γ (keV)	I_γ (%)	E_{ini} (keV)	Transition	Shell	α_{exp}	Mult. 1 (%)	Mult. 2 (%)
983.7		1919.9	$3^- \to 3^+$	K	$\leqslant 0.004$	$M1 \leqslant 10$	**E1**
996.3	50 (20)	1624.7	$6^- \to 5^+$	K	$\leqslant 0.004$	$M1 \leqslant 10$	**E1**
995.1	50 (20)	1919.9	$3^- \to 2^+$				
1006.2 $\geqslant 90$		1069.1	$3^+ \to 4^+$	K	0.0138(16)	**M1**	$E2 \leqslant 30$
				L	0.0024(4)	**M1**	$E2 \leqslant 40$
1033.3		1033.2	$4^+ \to 5^+$	K	0.0138(18)	**M1**	$E2 \leqslant 30$
				L	0.0022(3)	**M1**	$E2 \leqslant 40$
1095.0		1095.1	$6^+ \to 5^+$	K	0.014(5)	**M1**	$E2 \leqslant 40$
1101.6		2903.7	$\to$	K	0.009(5)	**M1**	$E2 \leqslant 100$
1169.1		1802.2	$1^+ \to 3^+$	K	0.0062(15)	$M1 \leqslant 60$	**E2**
1190.8		2126.8	$2^+ \to 3^+$	K	0.0071(14)	**M1**	$E2 \leqslant 70$
1239.1		2307.9	$4^- \to 3^+$	K	0.0015(4)		**E1**
1466.1		1529.4	$3^+ \to 4^+$	K	0.0045(10)	**M1**	$E2 \leqslant 80$
1476.5		1539.4	$2^+ \to 4^+$	K	0.0019(5)	$M1 \leqslant 30$	**E2**
1576.8 $\geqslant 80$		2501.6	$2^+ \to 2^+$	K	0.0026(7)	$M1 \leqslant 40$	**E2**
1640.4		1703.3	$5^- \to 4^+$	K	$\leqslant 0.0011$		**E1**

been derived from these as explained in the next section.

D. Levels and transition multipolarities

The low lying levels were recently critically reviewed by Boutachkov *et al.* [1]. In the following, we present additional evidence of the spin and parity assignments from the present conversion coefficient measurements.

In the γ-γ-coincidence measurements [1], it could be only indirectly verified that a transition went to the first excited state at 63 keV, because the 63.1 keV transition was below the electronic threshold for γ-ray detection in those measurements. Figure 4 shows the γ-ray spectrum from the present measurements, in coincidence with electrons in the 25–65 keV energy range, which contains the L, M, and N conversion lines of the 63 keV transition. This energy range also includes events of partial energy deposition due to backscattering from the Si(Li) detector. A corresponding sort of the data, projecting the electron spectrum with gates on γ rays that feed directly the 63 keV level shows that this (electron) window contains little background.

The γ spectrum of Fig. 4 essentially verifies the assignments of Ref. [1], since it clearly shows the lines that directly or indirectly proceed to the 63 keV state. The 569.9 keV transition, for example, is strong, while the 510.2 line is relatively reduced, the remaining intensity being largely from the positron annihilation line. Similarly, the 601.4 keV transition which is strong in Fig. 1 is essentially absent, leaving only the 602.9 keV line that feeds the 63 keV state.
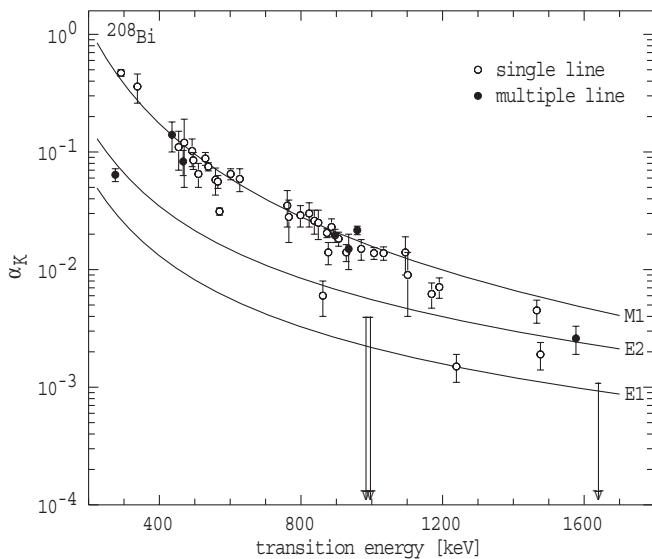

FIG. 2. Experimental K shell conversion coefficients of transitions in ^{208}Bi compared with calculations [12] for $E1$, $M1$, and $E2$ multipolarities.
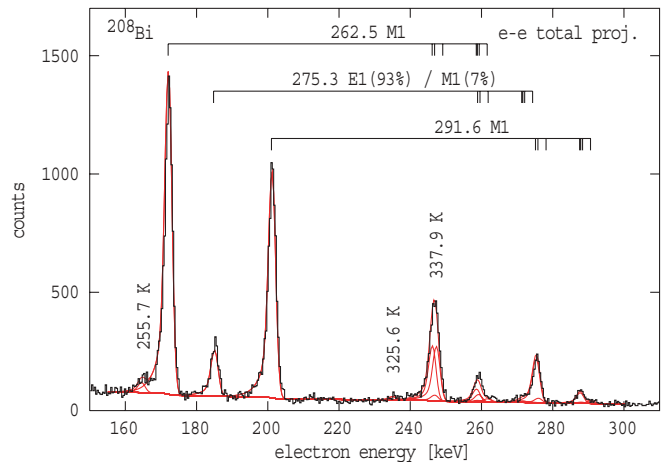

FIG. 3. (Color online) Total projection of e-e coincidences of ^{208}Bi. The experimental data are fitted with the calculated K, L, M lines for the indicated multipolarities.
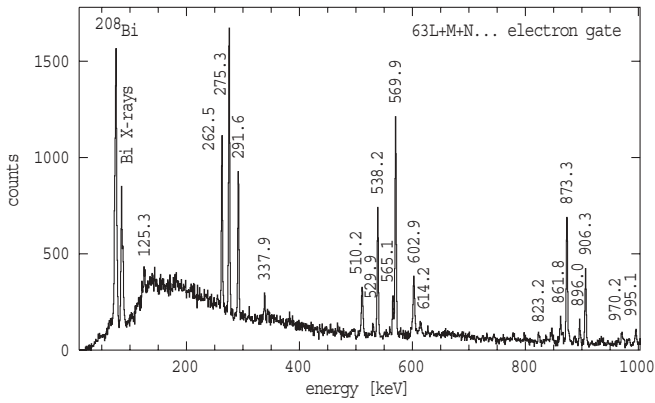
FIG. 4. γ rays in coincidence with conversion electrons $(L, M, N, \ldots)$ of the 63.1 keV transition from the first 4^+ level to the ground state.

Table I gives the multipolarities and mixing ratios as determined from the K and L shell conversion coefficients measured in lens mode. These results have been checked against the coincidence measurements and the few total conversion coefficients from Ref. [1]. Only $M1$ and either $E1$ or $E2$ multipolarity have been considered. Higher multipolarities are unimportant in the present context, and while $E0$ components could be present, there is insufficient evidence to consider them. Also, only two multipolarities can be considered for any transition; one is always taken as $M1$ and the other $E1$ or $E2$ depending on what is known about parities or from the magnitude of the measured coefficient. For a single transition, only pure $E1$ or mixed $M1/E2$ multipolarity is possible. But for unresolved multiplets, one transition might be $M1$ and another $E1$, as is clearly the case for the 275 keV doublet. For multiplets, column 2 of Table I gives the partition of the γ intensities from the data of Ref. [1]. The last columns give the multipolarities that result from the measured conversion coefficients. Usually, only the main multipolarity and a limit for the strength of the admixed component can be given. As the K conversion coefficient for $E2$ is only around 20% of that for $M1$, its strength can only be determined with a large error. It is unclear, why the point for the 1640 keV line falls below the value for $E1$.

The spin-parity of the lowest 14 levels below 1.2 MeV excitation energy had been firmly assigned before [1]. The present experimental conversion coefficients (Fig. 2) show the dominance of $M1$ transitions, in general agreement with those assignments. From the measured conversion coefficients, some $M1/E2$ mixing ratios, notably for the 510 and 570 keV lines, could be determined. The 565 keV line from the 628 keV, 5^+ level is also probably a mixed $M1/E2$ transition. The 862, 1169, and 1476 keV lines have to be pure $E2$ from the assigned spin differences, being nominally $2^+ \to 4^+$, $1^+ \to 3^+$, and $2^+ \to 4^+$, transitions, respectively. The measured conversion for the 862 keV line agrees with this, but the experimental values for the 1169 and 1476 keV lines both fall marginally (outside the quoted error) below the expected $E2$ values, indicating either different assignments or, more likely, additional systematic error.
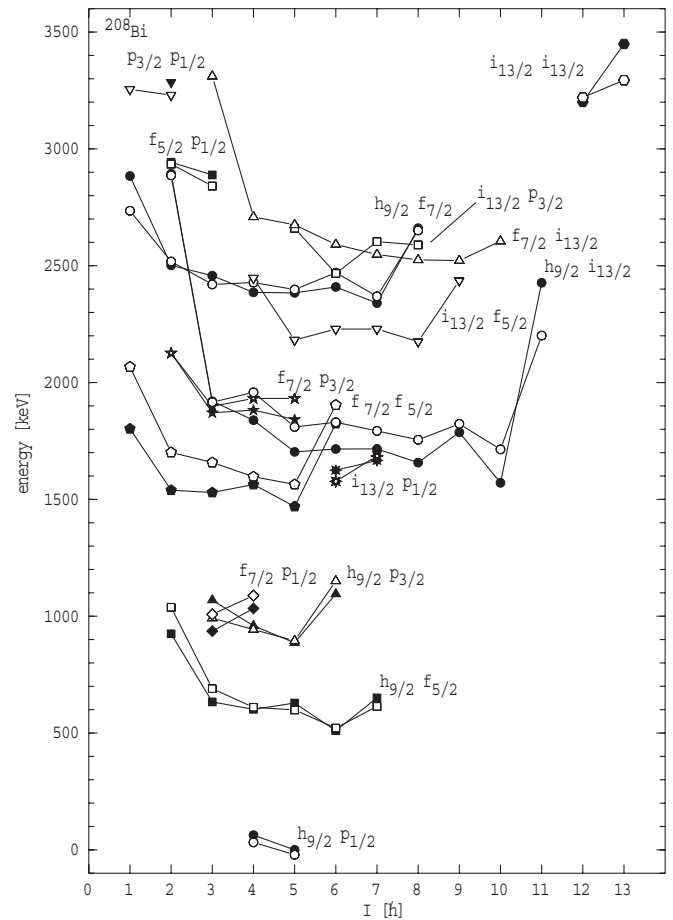
FIG. 5. Measured and calculated 1p-1h states in ^{208}Bi. The levels are grouped by their main configuration as indicated. Calculations have been performed with experimental single-particle energies and the H7B residual interaction. Filled (open) symbols indicate experimental (calculated) energies. Some symbols are used for two different configurations and are, however, clearly distinguished.

Up to an excitation energy of 1200 keV, only positive parity states could be reasonably expected, but according to the shell model calculations, between 1400 and 2200 keV states of either parity will be present in the spectrum. In this energy range, the negative parity states are populated by transfer reactions, but positive parity states are not (see Fig. 5). The two strong transitions at 436 and 959 keV from the 1469 keV level are both unresolved doublets in the experimental spectrum, but the large measured electron intensity for both transitions rules out either component of the doublet being an $E1$ and fixes the spin and parity of the 1469 keV as 5^+. Also, $M1$ components in some of the decays from the 1529, 1539, and 1564 keV levels determine their parity as positive. Similarly, from the observation of $M1$ decays, the 1802 keV level is 1^+, the 1871 keV level is 3^+, and the 1882 keV level is 4^+. Because the 996 keV line to the 5^+ level from the 1625 keV state is $E1$, this state can be associated with the 6^- member of the $\pi i_{13/2} \nu p_{1/2}$ configuration, and the 1667 keV level is then 7^-. The $\pi h_{9/2} \nu i_{13/2}$ decuplet has been seen in the pickup reaction [7]. The 1703 keV 5^- state decays by the 1640 keV $E1$ transition to a 4^+ state in agreement with the parity from

the $l = 6$ pickup. The 1715.5 and 1716.2 keV doublet agrees with the 6^-, 7^- assignment from transfer, but it is not possible to decide on the specific order.

For the eight known states of the $\pi h_{9/2} \nu f_{7/2}$ configuration, the multipolarity of the 1576 keV line from the 2501 keV level has been measured as $M1/E2$ or pure $E2$, in agreement with its $2^+ \rightarrow 2^+$ assignment. The $M1/E2$ assignment for the 1101 keV transition means that the 2904 keV level is $(0$–$3)^+$. The only expected positive parity state, which has not yet been identified around this energy, is the lowest 1p-1h 0^+ level. Negative parity can be assigned to the levels at 2308.0, 2478.4, 2570.2, 2657.3, 2718.5, 2838.9, and 2843.3 keV.

III. THE SHELL MODEL RESIDUAL INTERACTION

A. Data for determining the interaction

From the analysis of the level scheme by Boutachkov *et al.* [1] and the confirmation of spins and parities by the present conversion electron measurement, the one-particle one-hole states shown in Fig. 5 can be identified. All states belonging to 11 configurations are known, with two exceptions: only one experimental level has been seen that might be either from the $(\pi f_{7/2} \nu p_{3/2}; 5^+)$ configuration or much more likely from the $(\pi f_{7/2} \nu f_{5/2}; 6^+)$ configuration, and the 1^+ level of the $\nu p_{3/2} \nu p_{1/2}$ configuration is missing. Also the 12^+ and 13^+ states of the $\pi i_{13/2} \nu i_{13/2}$ configuration are known [13]. These 51 states are listed in Table II. The level energies comprise one set of data, which has to be fitted in the comparison with theory.

Measured states have been taken to be of 1p-1h structure on the following considerations: (i) strong population occurs in transfer reactions, (ii) no 2p-2h levels are expected below 2 MeV excitation energy, and (iii) 2p-2h states with positive parity will only occur above 3 MeV. These requirements clearly distinguish between 1p-1h and 2p-2h states.

1. Spectroscopic factors

The proton stripping reaction ^{207}Pb(^{3}He,d)^{208}Bi and the neutron pickup reactions ^{209}Bi(p, d)^{208}Bi and ^{209}Bi(d, t) have been thoroughly studied [5,6]. The results of the two neutron pickup studies agree very well. The measured spectroscopic factors are presented in Table II. Unresolved doublets had been claimed for some cases in these transfer reactions, because the measured strength was too large for a single state. These doublets have now been resolved in the γ-ray measurements, and their assigned spins agree with the summed strength for approximately pure configurations. Unfortunately, no uncertainties on the spectroscopic factors were given in the original publications, forcing us to estimate the errors, judging from the published data, as they are needed to give weights for the fitting.

The transfer reaction measurements were extensive and essentially complete, therefore if levels that have now been identified had not been observed in transfer, it can be concluded that the corresponding spectroscopic factors are small or vanish. They have been set to zero in the present fits with

an error of 10% of the full possible strength. In effect, this adds many more data points. For instance, a 4^+ level can be populated by $l = 3$ and $l = 5$ proton transfer to the $p_{1/2}^{-1}$ ground state of ^{207}Pb and neutron pickup from the $h_{9/2}$ ground state of ^{209}Bi with $l = 1$ and $l = 3$. If this state is not observed, all four spectroscopic factors are zero, meaning that the probabilities of the corresponding six configurations in this state are all small; its main configuration is therefore restricted to the two remaining possibilities: $\pi f_{7/2} \nu p_{3/2}$ or $\pi f_{7/2} \nu f_{5/2}$.

2. M1 and E2 matrix elements

To calculate the strength of γ transitions, the $M1$ and $E2$ matrix elements for single particles are needed. Transitions of other multipolarities are rare and cannot be calculated. Table III shows the elements for all orbitals of the Kuo-Herling space that have been used. It is an updated version of the data from Ref. [14] including some more recent measurements. Measured elements are used where available, and this is the case for the most important moments of the low lying orbitals. Where these are not available, calculated [15,16] values have been used. As we treat the states simply as 1p-1h, the electromagnetic moments must contain contributions from core polarization and mesonic effects. This is trivially fulfilled for measured moments, but it is also the case that calculations include them to some extent. Seven specific elements were not known well, but they have a significant influence on the γ transitions in ^{208}Bi. They have been fitted once to the present data and then kept constant for the fit of the residual interaction. It is a distinctive feature of the ^{208}Pb region that many electromagnetic moments have been precisely measured, and consequently γ transitions can be calculated reliably.

3. γ-branching ratios

A selection of the measured γ-branching ratios from Boutachkov *et al.* [1] are presented in Table IV. This table contains only states that are assigned as 1p-1h excitations and the γ-ray transitions between them, the 2p-2h states being irrelevant for the present analysis. A few corrections have been made to erroneous values of Ref. [1] as marked in the table. As is the case for the spectroscopic factors, the measurement of γ-ray transitions is considered to be complete. Therefore unobserved transitions are taken to have branching ratios of zero, with an error of 10% of the strongest transition from the particular level. Also, in Ref. [1] the primary concern was to list only safely assigned transitions, but in the present case a few examples of candidate lines that are only seen in single ? (and could only be observed in singles) have also been placed and included.

B. Proton neutron hole interaction

1. Procedure for determining the interaction

The states of ^{208}Bi are described as a superposition of proton-particle, neutron-hole configurations, that is,

$$\psi = \sum_{i=1}^{m} a_i |pn_i\rangle, \quad (1)$$

TABLE II. Measured energies, spins, main configurations, and spectroscopic factors of one-proton one-neutron-hole states in ^{208}Bi as used to fit the residual interaction. S_{calc} has been calculated with the fitted interaction. (See text for more explanation.)

E (keV)	J^π	Configuration	Proton transfer			Neutron pickup		
			l value	S_{exp}	S_{calc}	l value	S_{exp}	S_{calc}
0.0	5^+	$\pi h_{9/2} \nu p_{1/2}^{-1}$	5	5.25(25)	5.37	1	1.07(7)	1.076
63.1	4^+	$\pi h_{9/2} \nu p_{1/2}^{-1}$	5	4.1(3)	4.473	1	0.87(5)	0.898
510.2	6^+	$\pi h_{9/2} \nu f_{5/2}^{-1}$				3	1.3(1)	1.28
601.4	4^+	$\pi h_{9/2} \nu f_{5/2}^{-1}$				3	0.8(1)	0.825
628.3	5^+	$\pi h_{9/2} \nu f_{5/2}^{-1}$	5	0.4(4)	0.097	3	1.1(1)	1.044
633.1	3^+	$\pi h_{9/2} \nu f_{5/2}^{-1}$	3	0.11(11)	0.10	3	0.7(1)	0.64
650.5	7^+	$\pi h_{9/2} \nu f_{5/2}^{-1}$				3	1.4(1)	1.497
886.4	5^+	$\pi h_{9/2} \nu p_{3/2}^{-1}$				1	1.02(10)	1.057
924.8	2^+	$\pi h_{9/2} \nu f_{5/2}^{-1}$				3	0.48(5)	0.467
936.2	3^+	$\pi f_{7/2} \nu p_{1/2}^{-1}$	3	3.4(1)	3.286			
959.0	4^+	$\pi h_{9/2} \nu p_{3/2}^{-1}$				1	0.79(11)	0.765
1033.2	4^+	$\pi f_{7/2} \nu p_{1/2}^{-1}$	3	3.9(6)	3.606	1	0.11(6)	0.067
1069.1	3^+	$\pi h_{9/2} \nu p_{3/2}^{-1}$				1	0.64(6)	0.653
1095.1	6^+	$\pi h_{9/2} \nu p_{3/2}^{-1}$				1	1.19(11)	1.279
1469.4	5^+	$\pi f_{7/2} \nu f_{5/2}^{-1}$						
1529.4	3^+	$\pi f_{7/2} \nu f_{5/2}^{-1}$	3	0.0(1)	0.024			
1539.4	2^+	$\pi f_{7/2} \nu f_{5/2}^{-1}$	3	0.0(2)	0.001			
1563.5	4^+	$\pi f_{7/2} \nu f_{5/2}^{-1}$	3	0.18(5)	0.177			
1570.8	10^-	$\pi h_{9/2} \nu i_{13/2}^{-1}$				6	2.1(2)	2.089
1624.7	6^-	$\pi i_{13/2} \nu p_{1/2}^{-1}$	6	5.9(5)	6.221	6	0.1(1)	0.041
1657.4	8^-	$\pi h_{9/2} \nu i_{13/2}^{-1}$				6	1.7(2)	1.684
1666.5	7^-	$\pi i_{13/2} \nu p_{1/2}^{-1}$	6	5.6(5)	6.088			
1703.3	5^-	$\pi h_{9/2} \nu i_{13/2}^{-1}$				6	1.1(1)	1.052
1715.5	6^-	$\pi h_{9/2} \nu i_{13/2}^{-1}$	6	1.1(11)	0.170	6	1.3(2)	1.235
1716.2	7^-	$\pi h_{9/2} \nu i_{13/2}^{-1}$	6	1.1(11)	0.756	6	1.5(2)	1.265
1787[a]	9^-	$\pi h_{9/2} \nu i_{13/2}^{-1}$				6	1.9(2)	1.870
1802.2	1^+	$\pi f_{7/2} \nu f_{5/2}^{-1}$	1	0.0(2)	0.04			
1824.3	6^+	$\pi f_{7/2} \nu f_{5/2}^{-1}$				3	0.0(2)	0.001
1838.9	4^-	$\pi h_{9/2} \nu i_{13/2}^{-1}$				6	0.9(2)	0.856
1842[b]	5^+	$\pi f_{7/2} \nu p_{3/2}^{-1}$	5	0.0(4)	0.003			
1870.7	3^+	$\pi f_{7/2} \nu p_{3/2}^{-1}$						
1882.1	4^+	$\pi f_{7/2} \nu p_{3/2}^{-1}$	3	0.3(1)	0.194			
1919.9	3^-	$\pi h_{9/2} \nu i_{13/2}^{-1}$				6	0.7(1)	0.674
2126.8	2^+	$\pi f_{7/2} \nu p_{3/2}^{-1}$	1	0.08(4)	0.074			
2340.0	7^+	$\pi h_{9/2} \nu f_{7/2}^{-1}$				3	1.44(10)	1.424
2383.8	4^+	$\pi h_{9/2} \nu f_{7/2}^{-1}$				3	1.0(2)	0.787
2386.0	5^+	$\pi h_{9/2} \nu f_{7/2}^{-1}$				3	1.0(2)	0.899
2409.0	6^+	$\pi h_{9/2} \nu f_{7/2}^{-1}$				3	1.3(1)	1.277
2413[a]	9^-	$\pi i_{13/2} \nu f_{5/2}^{-1}$				6	0.00(95)	0.012
2427[a]	11^-	$\pi h_{9/2} \nu i_{13/2}^{-1}$				6	2.3(2)	2.297
2457.3	3^+	$\pi h_{9/2} \nu f_{7/2}^{-1}$	3	0.17(10)	0.103	3	0.7(1)	0.546
2475[a]	9^-	$\pi f_{7/2} \nu i_{13/2}^{-1}$				6	0.00(95)	0.009
2501.6	2^+	$\pi h_{9/2} \nu f_{7/2}^{-1}$				3	0.45(5)	0.423

TABLE II. (*Continued.*)

E (keV)	J^π	Configuration	Proton transfer			Neutron pickup		
			l value	S_{exp}	S_{calc}	l value	S_{exp}	S_{calc}
2660.6	8^+	$\pi h_{9/2} \nu f_{7/2}^{-1}$				3	1.55(15)	1.550
2884.0	1^+	$\pi h_{9/2} \nu f_{7/2}^{-1}$				3	0.30(5)	0.273
2888.5	3^+	$\pi f_{5/2} \nu p_{1/2}^{-1}$	3	3.4(3)	3.216			
2893.7	2^-	$\pi h_{9/2} \nu i_{13/2}^{-1}$				6	0.23(5)	0.466
2942.9	2^+	$\pi f_{5/2} \nu p_{1/2}^{-1}$	3	2.8(3)	2.149			
3201[a]	12^+	$\pi i_{13/2} \nu i_{13/2}^{-1}$						
3285.0	2^+	$\pi p_{3/2} \nu p_{1/2}^{-1}$	1	1.68(20)	1.682			
3449[a]	13^+	$\pi i_{13/2} \nu i_{13/2}^{-1}$						

[a]State has not been seen in the present study or Ref. [1].
[b]"Dummy" level, only one level has been observed at 1824.3 keV, which might be the 6^+ as assumed here or the 5^+.

where pn_i stands for the combination of any of the proton orbitals of the major shell between 82 and 126 and of the neutron holes in the same range. This encompasses the space of $h_{9/2}$, $f_{7/2}$, $f_{5/2}$, $p_{3/2}$, $p_{1/2}$, and $i_{13/2}$ orbitals. The 2p-2h components are not considered.

The number of possible particle-hole components m has a maximum of $m = 21$ for the 3^+ state. A level is completely described by the set of amplitudes a_i and its energy. Of course, the wave functions for all levels of I^π have to be orthonormal. All observable properties can be calculated from the wave functions and the operators corresponding to the observables. These involve the $M1$ and $E2$ operators defined by their matrix elements in Sec. III A, while the energies and spectroscopic factors are easily calculated.

The wave functions can be calculated by diagonalizing the Hamilton operator given by the single-particle energies and the residual two-body interaction. The single-particle energies are taken from experiment [1], while the residual interaction can be calculated from the various parametrizations of the measured interaction between free nucleons. Here we take an interaction based on the H7B parametrization [20] as a starting point. It has been converted to a particle-hole interaction by the Pandya transformation [21] from the primary particle-particle scheme. The goal is to determine as many elements of the residual interaction as possible from a fit to the experimental data of ^{208}Bi. These fitted elements are then substituted for the original H7B elements, while those H7B elements that are not sensitive to the experimental data are retained.

In previous work [14,22], the amplitudes of the wave functions were adjusted by trial and error to fit the measured γ decay. This procedure for the determination of the wave functions has the advantage that the dependence of the γ decay on the wave functions is sufficiently transparent that the appropriate direction of variation of the wave function amplitudes is intuitive and a reasonable fit can be achieved by trial and error. Once the energies and wave functions, the amplitudes, of the states are determined in this way, the Hamiltonian can be calculated straightforwardly from a set of linear equations. However, the trial and error approach becomes impractical for larger data sets. Also, after each

change of one wave function, the complete set for one I^π has to be orthonormalized, which might change properties in an unexpected manner, rendering the approach difficult.

In the present study, we have used an automatic nonlinear least-squares fit to handle the large set of data. Fitting of the amplitudes of the wave functions is still difficult because of the orthonormality constraint. However, the orthonormality requirement of the wave functions is equivalent to the symmetry requirement of the Hamiltonian $H_{ik} = H_{ki}$, which is trivial to obey. Therefore it is easier to start directly from the Hamiltonian and optimize its matrix elements. The nuclear properties that are to be compared with experiment are calculated from the Hamiltonian, with the wave functions as an intermediate step, and the elements of the residual interaction varied for the best fit.

Only positive parity states have been treated. There are few low lying negative parity states, and they decay primarily by $E1$ transitions, which are forbidden in the configuration space considered and therefore cannot be calculated. Fitting of the interaction is helped by the fact that one configuration tends to dominate for each state, and mixing with much higher lying levels is small. Therefore, if m levels were known from experiment for a given I^π, then the $[(m+1)(m+2)/2 - 1]$ elements of the submatrix for the corresponding m configurations and the next higher were fitted; the diagonal element of the highest configuration was left unchanged. In total, 150 elements out of 976 for spin 1^+ to 8^+ have been fitted. There is insufficient information to fit the interaction with still higher lying configurations, and so the original, unchanged H7B elements have been used for these.

Up to 80 parameters were optimized simultaneously with the nonlinear least-squares fitting routine FIT77. The data to be reproduced were the level energies, spectroscopic factors, nd γ-branching ratios. Of course, the interaction is diagonal in spin and parity, and the level energies and spectroscopic factors depend only on the elements of the interaction for this spin and parity. However, $M1$ transitions proceed to neighboring spins, and $E2$ transitions connect states differing by up to 2 units of spin. Obviously, parity does not change for these transitions, and it turns out that $M1$ transitions are much more important

TABLE III. Reduced $M1$ (nm) and $E2$ ($e\mathrm{fm}^2$) single-particle elements used in the present calculations. The elements for holes are with the signs for holes, meaning for $E2$ the sign is reversed from that for particles. If initial and final orbitals are reversed, there is a sign $(-1)^{(I_{\mathrm{ini}} - I_{\mathrm{fin}})}$ for all elements.

From	To	$\langle|M1|\rangle$	$\langle|E2|\rangle$
$\pi 1g_{7/2}$	$\pi 1g_{7/2}$	4.69[d]	43.1[d]
	$\pi 2d_{5/2}$	0.23[d]	13.8[d]
	$\pi 2d_{3/2}$		51.8[d]
$\pi 2d_{5/2}$	$\pi 2d_{5/2}$	5.931[a]	40.11[a]
	$\pi 2d_{3/2}$	1.901[a]	−20.51[a]
	$\pi 3s_{1/2}$		37.11[a]
$\pi 2d_{3/2}$	$\pi 2d_{3/2}$	0.961[a]	29.61[a]
	$\pi 3s_{1/2}$	0.301[a]	33.51[a]
$\pi 1h_{11/2}$	$\pi 1h_{11/2}$	12.714	67.02[b]
$\pi 1h_{9/2}$	$\pi 1h_{9/2}$	6.971[a]	−55.91[a]
	$\pi 2f_{7/2}$	0.181[a]	−15.51[a]
	$\pi 2f_{5/2}$		−71.0[e]
$\pi 2f_{7/2}$	$\pi 2f_{7/2}$	8.08[f]	−61.4[f]
	$\pi 2f_{5/2}$	−1.90[e]	−19.9[d]
	$\pi 3p_{3/2}$		54.4[d]
$\pi 2f_{5/2}$	$\pi 2f_{5/2}$	2.42[d]	−46.5[d]
	$\pi 3p_{3/2}$		20.0[d]
	$\pi 3p_{1/2}$		38.7[d]
$\pi 3p_{3/2}$	$\pi 3p_{3/2}$	3.95[d]	−32.4[d]
	$\pi 3p_{1/2}$	−1.51[d]	−33.2[d]
$\pi 3p_{1/2}$	$\pi 3p_{1/2}$	−0.10[d]	
$\pi 1i_{13/2}$	$\pi 1i_{13/2}$	15.711[a]	−68.01[a]
$\nu 1h_{9/2}$	$\nu 1h_{9/2}$	1.18[d]	30.4[d]
	$\nu 2f_{7/2}$	0.24[d]	−8.4[d]
	$\nu 2f_{5/2}$		−44.3[d]
$\nu 2f_{7/2}$	$\nu 2f_{7/2}$	−2.011[a]	48.51[a]
	$\nu 2f_{5/2}$	−2.01[g]	−11.9[g]
	$\nu 3p_{3/2}$		26.6[i]
$\nu 2f_{5/2}$	$\nu 2f_{5/2}$	1.081[a]	25.91[a]
	$\nu 3p_{3/2}$	−0.441[a]	11.21[a]
	$\nu 3p_{1/2}$		20.61[a]
$\nu 3p_{3/2}$	$\nu 3p_{3/2}$	−1.48[h]	35.6[h]
	$\nu 3p_{1/2}$	−1.281[a]	−15.61[a]
$\nu 3p_{1/2}$	$\nu 3p_{1/2}$	0.711[a]	
$\nu 1i_{11/2}$	$\nu 1i_{11/2}$	1.071[a]	−39.31[a]
	$\nu 2g_{9/2}$	−0.351[a]	−6.91[a]
	$\nu 2g_{7/2}$		−40.0[d]
$\nu 2g_{9/2}$	$\nu 2g_{9/2}$	−2.52[c]	−39.01[a]
	$\nu 2g_{7/2}$	−1.961[a]	11.7[d]
	$\nu 3d_{5/2}$		−32.91[a]
$\nu 2g_{7/2}$	$\nu 2g_{7/2}$	1.491[a]	−31.31[a]
	$\nu 3d_{5/2}$		−6.91[a]
	$\nu 3d_{3/2}$		−23.21[a]
$\nu 3d_{5/2}$	$\nu 3d_{5/2}$	−1.901[a]	−18.11[a]
	$\nu 3d_{3/2}$	−1.631[a]	9.41[a]
	$\nu 4s_{1/2}$		−17.71[a]

TABLE III. (*Continued.*)

From	To	$\langle|M1|\rangle$	$\langle|E2|\rangle$
$\nu 3d_{3/2}$	$\nu 3d_{3/2}$	1.121[a]	−14.11[a]
	$\nu 4s_{1/2}$	−0.31[d]	−14.11[a]
$\nu 1j_{15/2}$	$\nu 1j_{15/2}$	−2.681[a]	−64.01[a]

[a]From Ref. [14].
[b]From Ref. [17].
[c]From Ref. [18].
[d]Calculated for $M1$ by R. Bauer *et al.* [16] and for $E2$ by P. Ring *et al.* [15].
[e]$\langle f_{5/2} \| E2 \| h_{9/2}\rangle$ has been adjusted by a factor of 1.13 and $\langle f_{5/2} \| M1 \| f_{7/2}\rangle$ by $1/1.13$ to fit the branching ratio from the 2826 keV $f_{5/2}$ level in ^{209}Bi [19].
[f]$M1$ element changed to 8.08 from 8.01, and $E2$ element from −53.5 to −61.4 in fit of present data.
[g]$M1$ element changed to −2.01 from −1.98, and $E2$ element from −11.7 to −11.9 in fit of present data.
[h]$M1$ element changed to −1.48 from −1.60 and $E2$ element from 16.9 to 35.6 in fit of present data.
[i]$E2$ element changed to 26.6 from 27.7 in fit of present data.

than $E2$ ones. Interaction elements from different spins were fitted simultaneously.

In detail, the fit procedure was as follows. The quantity to be minimized was

$$10\,000 \times \sum (E^{\star}_{\mathrm{exp}} - E^{\star}_{\mathrm{calc}})^2 + \sum \left(\frac{S_{\mathrm{exp}} - S_{\mathrm{calc}}}{\Delta S_{\mathrm{exp}}}\right)^2$$
$$+ \sum \left(\frac{B^{\gamma}_{\mathrm{exp}} - B^{\gamma}_{\mathrm{calc}}}{\Delta B^{\gamma}_{\mathrm{calc}}}\right)^2, \tag{2}$$

with the level energies $E^{\star}$ in MeV, the spectroscopic factors S as in Table II, and the γ branches (B^{γ}) as a percentage. The sums extended over all clearly assigned experimental levels and their γ-ray decays. The very small experimental errors of excited state energies would weight them too heavily, hence the chosen weight of 10 000, corresponding to a 10 keV error, with which the energies are easily fitted to 1 keV accuracy. The spectroscopic factors include $j = l \pm 1/2$ for $l = 1, 3$. Weighting of the γ-branching ratios by the experimental errors emphasizes the role of weak branches with often small errors. This might not be appropriate in all cases, because it could be unrealistic to expect that very weak branches would be calculated precisely.

The calculations started with initial values from the H7B interaction matrix. The fit routine was told which elements to vary. In an iterative sequence, the fitted elements were used together with the unchanged terms as the starting point for the next optimization. This procedure was repeated with varied combinations of elements to be fitted until no further significant improvement was possible. First the wave functions and energies were calculated by diagonalizing the full interaction matrix. The $M1$ and $E2$ elements connecting the particle-hole configurations were calculated by standard

TABLE IV. Comparison of measured (B^γ_{Exp}) γ-branching ratios and calculated ones (B^γ_{Calc}) obtained using the fitted interaction. Transitions between 1p-1h states with measured or calculated γ-branching ratios $\geqslant 0.1\%$ are listed, normalized to 100 for the strongest transition. Only $M1$, $E2$, or mixed $M1 + E2$ multipolarities are considered. In the latter case, the calculated values for the $M1$ and $E2$ components are given separately. Erroneous branching ratios of Ref. [1] that have been corrected for the levels at 628.3, 1563.5, 2386.0, 2457.3, and 2884.0 keV by a reevaluation of the data of Ref. [1] are indicated by *italics*. The total calculated γ-transition rates from the levels are also given.

E_{ini} (keV)	J^π_{ini}	E_{fin} (keV)	J^π_{fin}	E_γ (keV)	Multi-polarity	B^γ_{calc}	B^γ_{exp}
63.1	4^+	0.0	5^+	63.1	$M1$	99.96	100
					$E2$	0.04	
					Total rate: 0.867E+08 s^{-1}		
510.2	6^+	0.0	5^+	510.2	$M1$	41.1	100 (9)
					$E2$	58.9	
		63.1	4^+	447.1	$E2$	6.11	7.2 (18)
					Total rate: 0.680E+10 s^{-1}		
601.4	4^+	0.0	5^+	601.4	$M1$	98.44	100 (9)
					$E2$	1.56	
		63.1	4^+	538.3	$M1$	51.7	54 (5)
					$E2$	1.72	
					Total rate: 0.170E+12 s^{-1}		
628.3	5^+	0.0	5^+	628.3	$M1$	21.1	
					$E2$	7.77	
		63.1	4^+	565.3	$M1$	87.7	100 (7)
					$E2$	12.3	
		510.2	6^+	118.2	$M1$	32.2	4.2 (12)
					$E2$	0.03	
		601.4	4^+	27.0	$M1$	0.46	*0.41(5)*
					$E2$	0.00	
					Total rate: 0.354E+11 s^{-1}		
633.1	3^+	0.0	5^+	633.1	$E2$	1.88	1.3 (2)
		63.1	4^+	570.0	$M1$	91.7	100 (6)
					$E2$	8.27	
		601.4	4^+	31.7	$M1$	0.26	2.4 (6)
					$E2$	0.00	
					Total rate: 0.519E+11 s^{-1}		
650.5	7^+	0.0	5^+	650.5	$E2$	100.	100 (20)
		510.2	6^+	140.3	$M1$	59.2	51 (13)
					$E2$	0.13	
					Total rate: 0.153E+11 s^{-1}		
886.4	5^+	0.0	5^+	886.4	$M1$	99.07	100 (20)
					$E2$	0.93	
		63.1	4^+	823.3	$M1$	64.2	78 (17)
					$E2$	0.40	
		510.2	6^+	376.2	$M1$	3.16	
					Total rate: 0.519E+13 s^{-1}		
924.8	2^+	63.1	4^+	862.6	$E2$	32.3	32.3 (6)
		633.1	3^+	292.6	$M1$	99.96	100 (10)
					$E2$	0.04	
					Total rate: 0.201E+12 s^{-1}		
936.2	3^+	0.0	5^+	936.2	$E2$	1.18	1.6 (4)
		63.1	4^+	873.1	$M1$	31.9	100 (6)
					$E2$	68.1	

TABLE IV. (*Continued.*)

E_{ini} (keV)	J_{ini}^{π}	E_{fin} (keV)	J_{fin}^{π}	E_{γ} (keV)	Multi-polarity	B_{calc}^{γ}	B_{exp}^{γ}
		601.4	4^+	334.8	$M1$	12.2	
		633.1	3^+	303.1	$M1$	1.14	1.3 (2)
					$E2$	0.00	
						Total rate: 0.187E+11 s^{-1}	
959.0	4^+	0.0	5^+	959.0	$M1$	44.6	40 (5)
					$E2$	1.47	
		63.1	4^+	895.9	$M1$	99.32	100 (10)
					$E2$	0.68	
		628.3	5^+	330.6	$M1$	1.32	2.9 (10)
					$E2$	0.01	
		633.1	3^+	325.9	$M1$	4.67	9.1 (15)
					$E2$	0.00	
						Total rate: 0.481E+13 s^{-1}	
1033.2	4^+	0.0	5^+	1033.2	$M1$	97.34	100 (6)
					$E2$	2.66	
		63.1	4^+	970.1	$M1$	76.4	45 (3)
					$E2$	0.82	
		601.4	4^+	431.8	$M1$	0.00	1.2 (3)
					$E2$	0.00	
		633.1	3^+	400.1	$M1$	0.37	2.3 (3)
					$E2$	0.01	
		886.4	5^+	146.8	$M1$	0.54	1.0 (2)
					$E2$	0.00	
						Total rate: 0.1284E+13 s^{-1}	
1069.1	3^+	0.0	5^+	1069.1	$E2$	0.37	2.8 (4)
		63.1	4^+	1006.0	$M1$	99.86	100 (6)
					$E2$	0.14	
		601.4	4^+	467.7	$M1$	6.65	9.0 (7)
					$E2$	0.00	
		633.1	3^+	436.0	$M1$	0.07	2.4 (3)
					$E2$	0.00	
		959.0	4^+	110.1	$M1$	0.43	0.6 (2)
					$E2$	0.00	
						Total rate: 0.572E+13 s^{-1}	
1095.1	6^+	0.0	5^+	1095.1	$M1$	99.71	100 (10)
					$E2$	0.29	
		886.4	5^+	208.7	$M1$	1.34	
						Total rate: 0.916E+13 s^{-1}	
1469.4	5^+	510.2	6^+	959.2	$M1$	94.90	100 (14)
					$E2$	5.10	
		601.4	4^+	868.0	$M1$	1.56	
		628.3	5^+	841.0	$M1$	7.64	9 (6)
					$E2$	1.65	
		959.0	4^+	510.4	$M1$	4.49	
		1033.2	4^+	436.2	$M1$	17.0	18 (4)
					$E2$	1.13	
						Total rate: 0.423E+12 s^{-1}	
1529.4	3^+	0.0	5^+	1529.4	$E2$	17.5	19 (5)
		63.1	4^+	1466.3	$M1$	39.5	49 (7)
					$E2$	3.15	
		601.4	4^+	928.0	$M1$	99.93	105 (11)

TABLE IV. (*Continued.*)

E_{ini} (keV)	J_{ini}^{π}	E_{fin} (keV)	J_{fin}^{π}	E_{γ} (keV)	Multi-polarity	B_{calc}^{γ}	B_{exp}^{γ}
					$E2$	0.07	
		628.3	5^+	901.0	$E2$	4.90	
		633.1	3^+	896.3	$M1$	38.7	44 (8)
					$E2$	3.20	
		924.8	2^+	603.7	$M1$	4.31	
		936.2	3^+	593.2	$M1$	13.7	17 (6)
					$E2$	2.03	
		959.0	4^+	570.4	$M1$	5.94	
		1033.2	4^+	496.2	$M1$	95.6	100 (12)
					$E2$	0.10	
		1069.1	3^+	460.3	$M1$	11.4	
						Total rate: 0.976E+12 s^{-1}	
1539.4	2^+	63.1	4^+	1476.3	$E2$	12.0	12.0 (8)
		601.4	4^+	938.0	$E2$	2.98	3.0 (2)
		633.1	3^+	906.3	$M1$	95.0	100 (6)
					$E2$	5.0	
		924.8	2^+	613.7	$M1$	5.68	7.4 (5)
					$E2$	0.33	
		936.2	3^+	603.2	$M1$	18.4	20.3 (12)
					$E2$	2.33	
		1069.1	3^+	470.3	$M1$	3.0	3.0 (2)
					$E2$	0.00	
						Total rate: 0.283E+12 s^{-1}	
1563.5	4^+	0.0	5^+	1563.5	$M1$	23.0	
		510.2	6^+	1053.4	$E2$	1.70	
		601.4	4^+	962.2	$M1$	2.13	
		628.3	5^+	935.2	$M1$	62.9	67 (14)
					$E2$	2.86	
		633.1	3^+	930.5	$M1$	5.10	
		886.4	5^+	677.2	$M1$	3.75	*3 (1)*
					$E2$	0.35	
		936.2	3^+	627.4	$M1$	99.02	100 (20)
					$E2$	0.98	
		1033.2	4^+	530.4	$M1$	12.46	25 (8)
					$E2$	0.11	
		1069.1	3^+	494.5	$M1$	1.56	1.7 (10)
					$E2$	0.00	
						Total rate: 0.166E+13 s^{-1}	
1657.4	8^-	1570.8	10^-	86.6	$E2$	100.	
						Total rate: 0.142E+05 s^{-1}	
1666.5	7^-	1624.7	6^-	41.8	$M1$	100.	
		1657.4	8^-	9.1	$M1$	6.66	
						Total rate: 0.555E+08 s^{-1}	
1703.3	5^-	1624.7	6^-	78.6	$M1$	100.	
						Total rate: 0.923E+09 s^{-1}	
1715.5	6^-	1624.7	6^-	90.8	$M1$	100.	
		1666.5	7^-	49.0	$M1$	9.73	
		1703.3	5^-	12.2	$M1$	1.19	
						Total rate: 0.714E+10 s^{-1}	

TABLE IV. (*Continued.*)

E_{ini} (keV)	J_{ini}^{π}	E_{fin} (keV)	J_{fin}^{π}	E_{γ} (keV)	Multi-polarity	B_{calc}^{γ}	B_{exp}^{γ}
1716.2	7^-	1624.7	6^-	91.5	$M1$	15.9	
		1657.4	8^-	58.8	$M1$	100.	
						Total rate: 0.722E+10 s^{-1}	
1787	9^-	1570.8	10^-	216.2	$M1$	99.9	
		1657.4	8^-	129.6	$M1$	37.3	
						Total rate: 0.185E+12 s^{-1}	
1802.2	1^+	633.1	3^+	1169.0	$E2$	10.0	6.8 (4)
		924.8	2^+	876.4	$M1$	17.7	17.3 (10)
					$E2$	0.06	
		936.2	3^+	865.9	$E2$	19.1	16.3 (10)
		1539.4	2^+	262.7	$M1$	99.97	100 (5)
					$E2$	0.03	
						Total rate: 0.645E+12 s^{-1}	
1824.3	6^+	0.0	5^+	1824.3	$E2$	1.88	
		510.2	6^+	1314.1	$M1$	9.68	
					$E2$	7.22	
		650.5	7^+	1173.8	$M1$	16.4	
					$E2$	21.0	
		886.4	5^+	937.9	$M1$	1.57	
		1033.2	4^+	791.1	$E2$	4.99	
		1095.1	6^+	729.2	$M1$	5.80	
		1469.4	5^+	354.9	$M1$	99.41	100 (8)
				354.9	$E2$	0.59	
						Total rate: 0.553E+12 s^{-1}	
1838.9	4^-	1703.3	5^-	135.6	$M1$	99.99	100 (26)
					$E2$	0.01	
						Total rate: 0.136E+12 s^{-1}	
1842	5^+	0.0	5^+	1842.0	$M1$	3.66	
		63.1	4^+	1778.9	$M1$	22.5	
					$E2$	1.72	
		510.2	6^+	1331.8	$M1$	1.58	
		628.3	5^+	1213.6	$M1$	10.8	
		959.0	4^+	883.0	$M1$	14.0	
		1033.2	4^+	808.8	$M1$	99.98	
		1563.5	4^+	278.4	$M1$	5.95	
						Total rate: 0.523E+13 s^{-1}	
1870.7	3^+	0.0	5^+	1870.7	$E2$	7.27	
		63.1	4^+	1807.6	$M1$	11.1	
					$E2$	1.73	
		601.4	4^+	1269.3	$E2$	1.43	
		633.1	3^+	1237.6	$M1$	8.59	
		924.8	2^+	945.0	$M1$	15.8	15 (3)
					$E2$	0.00	
		936.2	3^+	934.5	$M1$	112.	70 (30)
					$E2$	0.19	
		1033.2	4^+	837.5	$M1$	99.84	100 (10)
					$E2$	0.16	
		1539.4	2^+	331.3	$M1$	2.08	5.5 (17)
					$E2$	0.00	

TABLE IV. (*Continued.*)

E_{ini} (keV)	J_{ini}^{π}	E_{fin} (keV)	J_{fin}^{π}	E_{γ} (keV)	Multi-polarity	$B_{\mathrm{calc}}^{\gamma}$	$B_{\mathrm{exp}}^{\gamma}$
		1563.5	4^+	307.1	$M1$	7.51	7.5 (18)
					$E2$	0.01	
						Total rate: 0.110E+14 s^{-1}	
1882.1	4^+	0.0	5^+	1882.1	$M1$	2.57	
		63.1	4^+	1819.0	$M1$	16.8	
		510.2	6^+	1371.9	$E2$	2.12	
		601.4	4^+	1280.7	$M1$	26.9	
		628.3	5^+	1253.7	$M1$	1.19	
		633.1	3^+	1249.0	$M1$	5.10	
		936.2	3^+	945.9	$M1$	99.76	100 (10)
					$E2$	0.24	
		959.0	4^+	923.1	$M1$	10.6	6 (2)
					$E2$	0.07	
		1033.2	4^+	848.9	$M1$	28.2	3.6 (18)
					$E2$	0.23	
		1069.1	3^+	813.0	$M1$	9.37	18.2 (11)
					$E2$	0.00	
		1469.4	5^+	412.7	$M1$	26.2	25 (4)
					$E2$	0.10	
		1529.4	3^+	352.7	$M1$	4.41	
						Total rate: 0.928E+13 s^{-1}	
1919.9	3^-	1838.9	4^-	81.0	$M1$	100.	5 (2)
					$E2$	0.00	
						Total rate: 0.3221E+11 s^{-1}	
2126.8	2^+	63.1	4^+	2063.7	$E2$	28.8	
		601.4	4^+	1525.4	$E2$	4.15	
		633.1	3^+	1493.7	$M1$	18.9	16.3 (13)
					$E2$	0.00	
		924.8	2^+	1201.1	$M1$	15.3	13.9 (11)
					$E2$	0.00	
		936.2	3^+	1190.6	$M1$	98.25	100 (7)
					$E2$	1.75	
		1033.2	4^+	1093.6	$E2$	4.73	4.4 (8)
		1069.1	3^+	1057.7	$M1$	0.03	3.5 (7)
					$E2$	0.38	
		1529.4	3^+	597.4	$M1$	19.4	13 (2)
					$E2$	0.09	
		1539.4	2^+	587.4	$M1$	11.5	
		1802.2	1^+	324.7	$M1$	1.95	
		1870.7	3^+	256.1	$M1$	14.0	13.7 (11)
					$E2$	0.00	
						Total rate: 0.818E+13 s^{-1}	
2340.0	7^+	510.2	6^+	1830.2	$M1$	99.94	100
					$E2$	0.06	
		650.5	7^+	1689.9	$M1$	21.84	
						Total rate: 0.578E+14 s^{-1}	
2383.8	4^+	601.4	4^+	1782.4	$M1$	91.2	190 (90)
					$E2$	0.28	
		628.3	5^+	1755.4	$M1$	5.09	31 (13)
					$E2$	0.42	
		633.1	3^+	1750.7	$M1$	98.54	100 (6)

TABLE IV. (*Continued.*)

E_{ini} (keV)	J_{ini}^{π}	E_{fin} (keV)	J_{fin}^{π}	E_{γ} (keV)	Multi-polarity	B_{calc}^{γ}	B_{exp}^{γ}
					$E2$	1.46	
		886.4	5^+	1497.4	$M1$	1.73	
		936.2	3^+	1447.6	$M1$	2.45	
		1033.2	4^+	1350.6	$M1$	13.5	
		1069.1	3^+	1314.7	$M1$	3.67	
		1870.7	3^+	513.1	$M1$	1.34	
		1882.1	4^+	501.7	$M1$	1.63	
						Total rate: 0.609E+14 s^{-1}	
2386.0	5^+	63.1	4^+	2322.9	$M1$	4.88	
		510.2	6^+	1875.8	$M1$	16.2	
		601.4	4^+	1784.6	$M1$	173.	*90(130)*
					$E2$	0.01	
		628.3	5^+	1757.6	$M1$	99.73	100 (9)
					$E2$	0.27	
		633.1	3^+	1752.9	$E2$	0.97	50 (50)
		886.4	5^+	1499.6	$M1$	6.28	
					$E2$	1.49	
		959.0	4^+	1427.0	$M1$	5.09	
					$E2$	2.11	
		1095.1	6^+	1290.9	$M1$	1.79	
		1529.4	3^+	856.6	$E2$	0.00	15 (5)
		1563.5	4^+	822.4	$M1$	4.93	
		1842	5^+	544.0	$M1$	1.25	
		1882.1	4^+	503.9	$M1$	1.14	
						Total rate: 0.499E+14 s^{-1}	
2409.0	6^+	0.0	5^+	2409.0	$M1$	4.19	
		510.2	6^+	1898.9	$M1$	40.3	
		628.3	5^+	1780.7	$M1$	99.70	100 (6)
					$E2$	0.30	
		650.5	7^+	1758.6	$M1$	6.49	
		886.4	5^+	1522.7	$E2$	1.43	
						Total rate: 0.685E+14 s^{-1}	
2413	9^-	1570.8	10^-	842.2	$M1$	94.44	
					$E2$	5.56	
		1657.4	8^-	755.6	$M1$	90.6	
		1787	9^-	626.0	$M1$	1.46	
						Total rate: 0.207E+12 s^{-1}	
2457.3	3^+	63.1	4^+	2394.2	$M1$	1.26	
		601.4	4^+	1855.9	$M1$	71.3	73 (6)
					$E2$	0.45	
		633.1	3^+	1824.2	$M1$	99.75	100 (8)
					$E2$	0.25	
		924.8	2^+	1532.6	$M1$	51.1	50 (4)
					$E2$	0.38	
		936.2	3^+	1521.1	$M1$	2.23	
		959.0	4^+	1498.3	$M1$	1.66	
		1033.2	4^+	1424.1	$M1$	1.35	
		1069.1	3^+	1388.2	$M1$	4.62	*6.6(17)*
					$E2$	0.47	
		1539.4	2^+	917.9	$M1$	24.2	27 (2)
					$E2$	0.07	
		1563.5	4^+	893.7	$M1$	1.68	

TABLE IV. (*Continued.*)

E_{ini} (keV)	J_{ini}^{π}	E_{fin} (keV)	J_{fin}^{π}	E_{γ} (keV)	Multi-polarity	B_{calc}^{γ}	B_{exp}^{γ}
		1882.1	4^+	575.2	$M1$	5.21	
						Total rate: 0.625E+14 s^{-1}	
2475	9^-	1570.8	10^-	904.2	$M1$	90.34	
					$E2$	9.66	
		1657.4	8^-	817.6	$M1$	87.0	
		1787	9^-	688.0	$M1$	40.2	
		2413	9^-	62.0	$M1$	1.89	
						Total rate: 0.404E+12 s^{-1}	
2501.6	2^+	63.1	4^+	2438.4	$E2$	9.30	
		601.4	4^+	1900.1	$E2$	6.19	
		633.1	3^+	1868.4	$M1$	108.	90 (20)
					$E2$	0.03	
		924.8	2^+	1575.8	$M1$	99.4	100 (20)
					$E2$	0.60	
		936.2	3^+	1565.3	$M1$	4.52	
		959.0	4^+	1542.5	$E2$	5.63	
		1069.1	3^+	1432.4	$M1$	5.35	20 (6)
					$E2$	8.20	
		1870.7	3^+	630.8	$M1$	4.61	
						Total rate: 0.227E+14 s^{-1}	
2660.6	8^+	650.5	7^+	2010.1	$M1$	98.63	100
					$E2$	1.37	
		1095.1	6^+	1565.5	$E2$	1.78	
						Total rate: 0.572E+14 s^{-1}	
2884.0	1^+	633.1	3^+	2250.9	$E2$	11.9	
		924.8	2^+	1958.3	$M1$	103.	*100(40)*
					$E2$	0.00	
		936.2	3^+	1947.8	$E2$	2.72	
		1069.1	3^+	1814.9	$E2$	165.	*140(30)*
		2501.6	2^+	382.5	$M1$	100.	*100(10)*
					$E2$	0.00	
						Total rate: 0.136E+14 s^{-1}	
2888.5	3^+	0.0	5^+	2888.5	$E2$	100.	100
		63.1	4^+	2825.4	$E2$	6.23	
		601.4	4^+	2287.1	$M1$	2.05	
		924.8	2^+	1962.8	$M1$	1.38	
		936.2	3^+	1952.3	$M1$	1.07	
		959.0	4^+	1929.5	$M1$	3.37	
		1033.2	4^+	1855.3	$M1$	15.9	
						Total rate: 0.259E+15 s^{-1}	
2893.7	2^-	1919.9	3^-	973.8	$M1$	99.98	100 (60)
					$E2$	0.02	
						Total rate: 0.521E+14 s^{-1}	
2942.9	2^+	63.1	4^+	2879.8	$E2$	100.	100
		633.1	3^+	2309.8	$M1$	2.00	
		936.2	3^+	2006.7	$M1$	39.2	
						Total rate: 0.258E+15 s^{-1}	

TABLE IV. (*Continued.*)

E_{ini} (keV)	J_{ini}^π	E_{fin} (keV)	J_{fin}^π	E_γ (keV)	Multi-polarity	B_{calc}^γ	B_{exp}^γ
3285.0	2^+	601.4	4^+	2683.6	$E2$	4.88	
		633.1	3^+	2651.9	$M1$	8.06	
		924.8	2^+	2359.3	$M1$	16.3	
		936.2	3^+	2348.8	$M1$	6.87	
					$E2$	10.60	
		959.0	4^+	2326.0	$E2$	22.1	
		1033.2	4^+	2251.8	$E2$	100.	
		1069.1	3^+	2215.9	$M1$	7.96	
					$E2$	1.17	
		1529.4	3^+	1755.6	$M1$	52.8	
					$E2$	1.24	
		1802.2	1^+	1482.9	$M1$	1.31	
		1870.7	3^+	1414.3	$M1$	11.1	
		1882.1	4^+	1402.9	$E2$	1.08	
		2126.8	2^+	1158.2	$M1$	4.89	
		2457.3	3^+	827.7	$M1$	5.76	
					Total rate: 0.625E+14 s^{-1}		
3449	13^+	3201	12^+	248.2	$M1$	99.95	
					$E2$	0.05	
					Total rate: 0.100E+12 s^{-1}		

Racah algebra from the single-particle elements. With these electromagnetic matrix elements then, the transition matrix element between two states was calculated; for this only the first 12 configurations were used, higher ones being unimportant. The γ-ray transition rate was computed with the experimental γ-ray energy. This is a convenience in the fit, because the γ-decay is essentially independent of the calculated energy from the first iteration on.

C. Results

1. Results of the fit

The fit procedure reproduces level energies and spectroscopic factors well and easily. Since each level energy is mainly influenced by the diagonal element of its dominant configuration, the fit procedure could, roughly speaking, just involve adjustment of this one matrix element after the mixing has been handled. Indeed, the fitted interaction reproduces the level energies to 1 keV accuracy. Nevertheless, configuration mixing also contributes significantly to the energies. The diagonal elements cannot be separately determined just from the level energies; it is necessary to also fit the nondiagonal elements to obtain the energy shift from mixing.

Since the spectroscopic factors are given by the squared amplitude of the contributing configurations, small admixed components are nearly always insignificant, and the spectroscopic factors are also easily fitted within their estimated error of about 10% (see Table II). While only the transferred orbital angular momentum can be determined in the transfer reaction, spin-orbit splitting is so large that there is little mixing between the $p_{1/2}$ and $p_{3/2}$ or $f_{5/2}$ and $f_{7/2}$ orbitals. The worst agreement

is for one of the highest states, the 2^+ level at 2.943 MeV; its spectroscopic factor for $l = 3$ transfer in (^{3}He,d) is calculated as 2.15 and measured as 2.8(3). In only six other of the 51 cases, disagreement was found to be just outside the quoted errors, but the errors are in any case, only estimates. The table lists only measured factors; for the many additional spectroscopic factors that have not been measured because they are too small, the calculations also give negligible values. The spectroscopic factors determine very clearly, or at least severely restrict, the main configurations of the states. On this firm basis, even small configuration mixing can then be determined from the γ-ray information.

Also, configuration mixing of the wave functions depends not only on the mixing matrix elements of the Hamiltonian, but also on the diagonal elements; this is evident in perturbation theory, as they determine the energy denominators.

The γ decay can be very sensitive to small admixtures of the wave functions and therefore the nondiagonal interaction elements. The transition matrix elements between two states described by their wave functions as

$$\psi = \sum_{i=1}^m a_i |\nu_i\rangle \quad (3)$$

and

$$\phi = \sum_{i=1}^l b_i |\mu_i\rangle \quad (4)$$

are

$$\langle\phi|M1 \text{ or } E2|\psi\rangle = \sum_{i,k} a_i b_k \langle\mu_k|M1 \text{ or } E2|\nu_i\rangle, \quad (5)$$

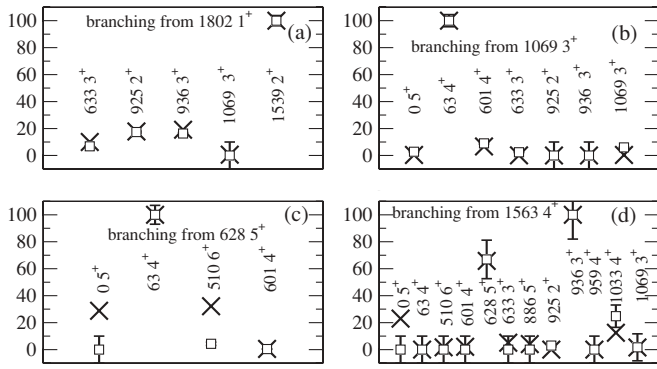where ν_i and μ_k are pure particle-hole configurations.

FIG. 6. Measured (squares with error bars) and calculated ($\times$) branching ratios for the decay from the (a) 1802.2 keV 1^+, (b) 1069.1 keV 3^+, (c) 628.3 keV 5^+, and (d) 1563.5 keV 4^+ levels in ^{208}Bi to the indicated states. The strongest transition is normalized to 100.

The sum contains many elements that might interfere constructively or destructively. Three extreme situations are presented in the following. One is if the transition between the main configurations is weak or even forbidden, and then small admixtures might be most important. Another is when two or three of the largest transition elements nearly cancel out. Finally, if a strong matrix element connects the main configurations of the initial and final states, this dominates, and smaller components become of little importance. The decay of the 5^+ state presented below illustrates these three extremes.

Table IV compares the measured branching ratios with those calculated by the fitted interaction. Only $M1$ and $E2$ transitions between 1p-1h states are included. Also, transitions are only shown if either they have been measured or the

calculated branch is greater than 0.1%. This leaves out many transitions that are unobserved and, accordingly, calculated to be of negligible intensity; they are, however, included in the fit. As an overall result indicating the value of the fit, the minimized quantity

$$\sum \left(\frac{B_{\text{exp}}^\gamma - B_{\text{calc}}^\gamma}{\Delta B_{\text{calc}}^\gamma} \right)^2 \qquad (6)$$

is lowered by a factor of 500, from 64 000 when the original H7B interaction is used, to 120 by the fit. This sum is over all positive parity states. The remaining summed-square error of 120 is mainly due to a few transitions that deviate significantly.

Table IV gives also the total calculated γ-transition rate from the levels. It indicates if the transitions are strong and therefore rather easy to reproduce, or weak and likely to be influenced by small components of the wave functions. A few cases are presented in more detail in Fig. 6. Five branches from the first 1^+ state at 1802 keV [Fig. 6(a)] are quite well reproduced, although the branches to the 3^+ levels at 633 and 936 keV are not within errors (Table IV). Similarly, the main features of the decay from the 1069 keV 3^+ level [Fig. 6(b)] are well fitted, but some small branches do not agree quantitatively. Of the 12 transitions from the 4^+ 1563 keV level, only one is clearly not reproduced [Fig. 6(d)].

The decay of the 5^+, 628 keV level [Fig. 6(c)] is an example in which good agreement would not be expected, as explained schematically in Fig. 7. The main contributions for the $M1$ transition to the ground state are from the main $h_{9/2} f_{5/2}$ component of the excited state to the same weak component of the ground state, and between the $h_{9/2} p_{1/2}$ configurations, which is weak in the initial level but strong in the ground state. These two matrix elements nearly cancel each other (Fig. 7), and a small change of either one would give
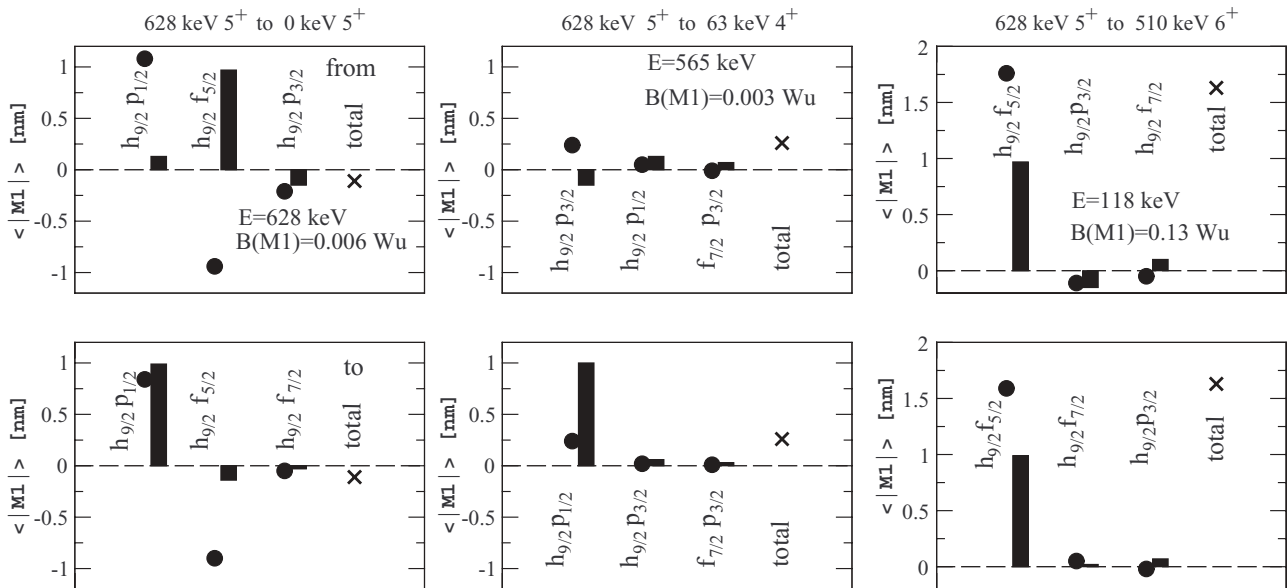

FIG. 7. $M1$ transition elements for the γ decays from the first excited 5^+ level at 628.3 keV in ^{208}Bi. The three configurations that contribute most to the transition are shown in the upper panels for the decaying state and in the lower panels for the populated level. The bars show the amplitude of the indicated configuration, the round dots the contribution to the transition element from this configuration, and x the total transition element.

a vastly different result. Because of this cancellation also, the small contributions from the other weak components become very important. The very small calculated $B(M1)$ value of 0.006 W.u. means that minute details of the structure can be decisive. In the second decay to the 4^+ state, the dominant $h_{9/2}f_{5/2}$ configuration of the 5^+ level contributes negligibly (less than the three very small components that are shown) to the decay, and the calculated $B(M1)$ is even smaller than that to the ground state. In contrast, the initial 5^+ state and the 6^+ level fed in the third decay both have $h_{9/2}f_{5/2}$ as the main configuration, that also dominate the transition. Therefore the calculated value should be reliable. Figure 6 shows that if theory and experiment had been normalized to this line instead of to the strongest, the branches to the 5^+ ground state and 601 keV 4^+ level would roughly agree. Only the weakest transition to the 63 keV 4^+ state with a calculated $B(M1) = 0.003$ W.u. would be badly reproduced.

2. *Results for the interaction*

The fitted interaction elements are compared with those from H7B in Table V. Figure 8 compares the diagonal elements with the proton in the $h_{9/2}$ orbital; while in Fig. 9, the proton is in the $f_{7/2}$ orbital. The trend as a function of spin shows the characteristic ∪ shape in agreement between calculated and fitted elements [23]. For the highest spin coupling, the rise is pronounced if spin and orbital angular momentum are parallel for the proton and antiparallel for the neutron hole or vice versa. The magnitude of the elements agrees also quite well.

There is a clear discrepancy for the 3^+ level of the diagonal $h_{9/2}f_{7/2}$ interaction where the fitted value is 250 keV larger than the H7B value. There is no obvious explanation for this, although these high lying configurations could be influenced by still higher lying unobserved configurations.

Figures 10–12 show the off-diagonal (mixing) elements. Again, calculated and fitted values agree reasonably well, although the mixing elements are quite small. As the range
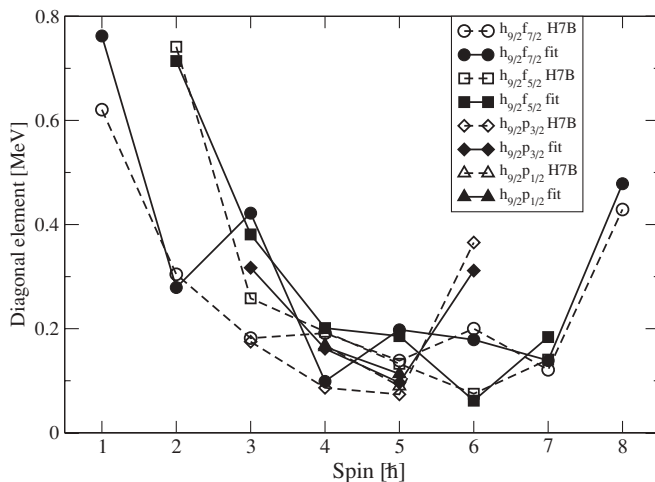

FIG. 8. Diagonal matrix elements of the interaction for configurations involving the $\pi h_{9/2}$ orbital. The open symbols mark the H7B interaction, the filled are from the fit.

TABLE V. Comparison of fitted and H7B interaction elements (MeV).

Matrix element	J	H7B	Fit
$\langle \pi 1h_{9/2}\nu 2f_{7/2}|H|\pi 1h_{9/2}\nu 2f_{7/2}\rangle$	1	0.621	0.762
	2	0.304	0.279
	3	0.182	0.422
	4	0.191	0.099
	5	0.138	0.198
	6	0.200	0.179
	7	0.121	0.139
	8	0.429	0.479
$\langle \pi 1h_{9/2}\nu 2f_{7/2}|H|\pi 1h_{9/2}\nu 2f_{5/2}\rangle$	2	−0.361	−0.460
	3	−0.003	−0.411
	4	−0.147	−0.094
	5	0.008	−0.173
	6	−0.114	−0.046
	7	0.049	0.104
$\langle \pi 1h_{9/2}\nu 2f_{7/2}|H|\pi 1h_{9/2}\nu 3p_{3/2}\rangle$	3	0.115	−0.099
	4	0.088	0.111
	5	0.056	0.143
	6	0.217	0.055
$\langle \pi 1h_{9/2}\nu 2f_{7/2}|H|\pi 1h_{9/2}\nu 3p_{1/2}\rangle$	4	−0.142	−0.053
	5	0.067	0.055
$\langle \pi 1h_{9/2}\nu 2f_{7/2}|H|\pi 2f_{7/2}\nu 2f_{7/2}\rangle$	2	−0.035	−0.295
	3	−0.015	0.557
	4	−0.034	0.013
	5	0.001	−0.324
	6	−0.031	0.028
	7	0.004	−0.214
$\langle \pi 1h_{9/2}\nu 2f_{7/2}|H|\pi 2f_{7/2}\nu 2f_{5/2}\rangle$	1	−0.041	0.179
	2	0.058	0.188
	3	−0.027	0.038
	4	0.030	−0.063
	5	−0.015	−0.010
	6	0.016	0.007
$\langle \pi 1h_{9/2}\nu 2f_{7/2}|H|\pi 2f_{7/2}\nu 3p_{3/2}\rangle$	2	0.081	−0.085
	3	0.048	−0.168
	4	−0.020	−0.109
	5	0.080	−0.141
$\langle \pi 1h_{9/2}\nu 2f_{7/2}|H|\pi 2f_{7/2}\nu 3p_{1/2}\rangle$	3	−0.091	−0.164
	4	0.041	−0.187
$\langle \pi 1h_{9/2}\nu 2f_{7/2}|H|\pi 2f_{5/2}\nu 3p_{1/2}\rangle$	2	−0.147	0.052
	3	0.087	−0.051
$\langle \pi 1h_{9/2}\nu 2f_{7/2}|H|\pi 3p_{3/2}\nu 3p_{1/2}\rangle$	1	−0.025	−0.021
	2	0.034	−0.044
$\langle \pi 1h_{9/2}\nu 2f_{7/2}|H|\pi 1i_{13/2}\nu 1i_{13/2}\rangle$	8	−0.129	−0.208
$\langle \pi 1h_{9/2}\nu 2f_{5/2}|H|\pi 1h_{9/2}\nu 2f_{5/2}\rangle$	2	0.742	0.714
	3	0.258	0.381
	4	0.194	0.201
	5	0.133	0.186
	6	0.075	0.062
	7	0.141	0.184
$\langle \pi 1h_{9/2}\nu 2f_{5/2}|H|\pi 1h_{9/2}\nu 3p_{3/2}\rangle$	3	0.093	0.178
	4	−0.106	−0.081
	5	0.057	0.029
	6	−0.131	−0.063

TABLE V. (*Continued.*)

| Matrix element	J	H7B	Fit
$\langle \pi 1h_{9/2}\nu 2f_{5/2}\|H\|\pi 1h_{9/2}\nu 3p_{1/2}\rangle$	4	0.112	0.011
	5	0.076	0.078
$\langle \pi 1h_{9/2}\nu 2f_{5/2}\|H\|\pi 2f_{7/2}\nu 2f_{7/2}\rangle$	2	0.098	−0.076
	3	−0.076	−0.498
	4	0.044	−0.268
	5	−0.051	0.234
	6	0.024	0.251
	7	−0.032	−0.097
$\langle \pi 1h_{9/2}\nu 2f_{5/2}\|H\|\pi 2f_{7/2}\nu 2f_{5/2}\rangle$	2	−0.015	0.007
	3	0.008	0.008
	4	0.017	−0.011
	5	−0.002	−0.013
	6	0.027	0.029
$\langle \pi 1h_{9/2}\nu 2f_{5/2}\|H\|\pi 2f_{7/2}\nu 3p_{3/2}\rangle$	2	0.115	0.222
	3	−0.042	0.034
	4	0.075	0.038
	5	0.007	−0.071
$\langle \pi 1h_{9/2}\nu 2f_{5/2}\|H\|\pi 2f_{7/2}\nu 3p_{1/2}\rangle$	3	0.039	0.056
	4	0.057	0.008
$\langle \pi 1h_{9/2}\nu 2f_{5/2}\|H\|\pi 2f_{5/2}\nu 3p_{1/2}\rangle$	2	0.269	0.178
	3	0.098	−0.315
$\langle \pi 1h_{9/2}\nu 2f_{5/2}\|H\|\pi 3p_{3/2}\nu 3p_{1/2}\rangle$	2	0.009	0.094
$\langle \pi 1h_{9/2}\nu 3p_{3/2}\|H\|\pi 1h_{9/2}\nu 3p_{3/2}\rangle$	3	0.175	0.317
	4	0.086	0.162
	5	0.074	0.096
	6	0.366	0.312
$\langle \pi 1h_{9/2}\nu 3p_{3/2}\|H\|\pi 1h_{9/2}\nu 3p_{1/2}\rangle$	4	−0.143	−0.061
	5	0.081	0.037
$\langle \pi 1h_{9/2}\nu 3p_{3/2}\|H\|\pi 2f_{7/2}\nu 2f_{7/2}\rangle$	3	−0.049	−0.347
	4	−0.016	−0.136
	5	−0.013	0.077
	6	−0.029	−0.204
$\langle \pi 1h_{9/2}\nu 3p_{3/2}\|H\|\pi 2f_{7/2}\nu 2f_{5/2}\rangle$	3	0.017	−0.027
	4	−0.004	0.069
	5	−0.001	−0.032
	6	−0.018	−0.035
$\langle \pi 1h_{9/2}\nu 3p_{3/2}\|H\|\pi 2f_{7/2}\nu 3p_{3/2}\rangle$	3	−0.024	0.036
	4	−0.011	0.040
	5	−0.003	0.039
$\langle \pi 1h_{9/2}\nu 3p_{3/2}\|H\|\pi 2f_{7/2}\nu 3p_{1/2}\rangle$	3	0.000	−0.012
	4	−0.005	0.022
$\langle \pi 1h_{9/2}\nu 3p_{3/2}\|H\|\pi 2f_{5/2}\nu 3p_{1/2}\rangle$	3	0.059	−0.136
$\langle \pi 1h_{9/2}\nu 3p_{1/2}\|H\|\pi 1h_{9/2}\nu 3p_{1/2}\rangle$	4	0.168	0.165
	5	0.090	0.113
$\langle \pi 1h_{9/2}\nu 3p_{1/2}\|H\|\pi 2f_{7/2}\nu 2f_{7/2}\rangle$	4	0.027	0.031
	5	−0.048	−0.113
$\langle \pi 1h_{9/2}\nu 3p_{1/2}\|H\|\pi 2f_{7/2}\nu 2f_{5/2}\rangle$	4	−0.001	−0.004
	5	0.009	−0.049
$\langle \pi 1h_{9/2}\nu 3p_{1/2}\|H\|\pi 2f_{7/2}\nu 3p_{3/2}\rangle$	4	0.011	−0.045
	5	−0.030	0.031
$\langle \pi 1h_{9/2}\nu 3p_{1/2}\|H\|\pi 2f_{7/2}\nu 3p_{1/2}\rangle$	4	0.008	−0.014
$\langle \pi 2f_{7/2}\nu 2f_{7/2}\|H\|\pi 2f_{7/2}\nu 2f_{5/2}\rangle$	2	0.097	−0.334
	3	−0.112	0.104
	4	0.143	−0.390
	5	−0.046	−0.047
	6	0.207	0.202
$\langle \pi 2f_{7/2}\nu 2f_{7/2}\|H\|\pi 2f_{7/2}\nu 3p_{3/2}\rangle$	2	0.196	0.530
	3	0.131	−0.487
	4	0.071	0.240
	5	0.147	−0.012
$\langle \pi 2f_{7/2}\nu 2f_{7/2}\|H\|\pi 2f_{7/2}\nu 3p_{1/2}\rangle$	3	−0.160	0.152
	4	0.130	0.113
$\langle \pi 2f_{7/2}\nu 2f_{7/2}\|H\|\pi 2f_{5/2}\nu 3p_{1/2}\rangle$	2	0.172	0.075
	3	−0.062	−0.008
$\langle \pi 2f_{7/2}\nu 2f_{7/2}\|H\|\pi 3p_{3/2}\nu 3p_{1/2}\rangle$	2	0.245	0.360
$\langle \pi 2f_{7/2}\nu 2f_{5/2}\|H\|\pi 2f_{7/2}\nu 2f_{5/2}\rangle$	1	1.219	0.918
	2	0.462	0.511
	3	0.340	0.217
	4	0.323	0.434
	5	0.210	0.114
	6	0.585	0.500
$\langle \pi 2f_{7/2}\nu 2f_{5/2}\|H\|\pi 2f_{7/2}\nu 3p_{3/2}\rangle$	2	0.177	0.265
	3	−0.088	0.019
	4	0.121	0.136
	5	−0.085	−0.080
$\langle \pi 2f_{7/2}\nu 2f_{5/2}\|H\|\pi 2f_{7/2}\nu 3p_{1/2}\rangle$	3	0.088	−0.007
	4	0.174	0.260
$\langle \pi 2f_{7/2}\nu 2f_{5/2}\|H\|\pi 2f_{5/2}\nu 3p_{1/2}\rangle$	2	−0.042	−0.001
	3	−0.055	0.160
$\langle \pi 2f_{7/2}\nu 2f_{5/2}\|H\|\pi 3p_{3/2}\nu 3p_{1/2}\rangle$	1	0.518	0.478
	2	0.266	0.224
$\langle \pi 2f_{7/2}\nu 3p_{3/2}\|H\|\pi 2f_{7/2}\nu 3p_{3/2}\rangle$	2	0.561	0.475
	3	0.193	0.339
	4	0.140	0.073
	5	0.252	0.161
$\langle \pi 2f_{7/2}\nu 3p_{3/2}\|H\|\pi 2f_{7/2}\nu 3p_{1/2}\rangle$	3	−0.178	−0.209
	4	0.231	0.119
$\langle \pi 2f_{7/2}\nu 3p_{3/2}\|H\|\pi 2f_{5/2}\nu 3p_{1/2}\rangle$	2	0.180	0.077
	3	−0.005	0.057
$\langle \pi 2f_{7/2}\nu 3p_{3/2}\|H\|\pi 3p_{3/2}\nu 3p_{1/2}\rangle$	2	0.215	0.294
$\langle \pi 2f_{7/2}\nu 3p_{1/2}\|H\|\pi 2f_{7/2}\nu 3p_{1/2}\rangle$	3	0.266	0.217
	4	0.398	0.363
$\langle \pi 2f_{7/2}\nu 3p_{1/2}\|H\|\pi 2f_{5/2}\nu 3p_{1/2}\rangle$	3	0.032	−0.049
$\langle \pi 2f_{5/2}\nu 3p_{1/2}\|H\|\pi 2f_{5/2}\nu 3p_{1/2}\rangle$	2	0.297	0.320
	3	0.131	0.098
$\langle \pi 2f_{5/2}\nu 3p_{1/2}\|H\|\pi 3p_{3/2}\nu 3p_{1/2}\rangle$	2	0.020	−0.037
$\langle \pi 3p_{3/2}\nu 3p_{1/2}\|H\|\pi 3p_{3/2}\nu 3p_{1/2}\rangle$	2	0.405	0.535
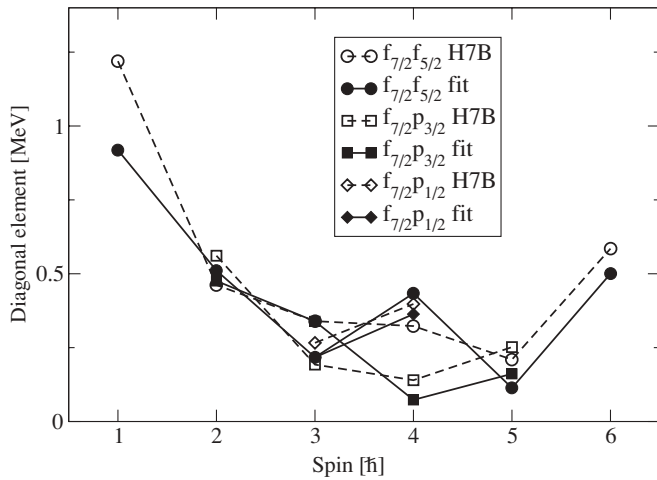
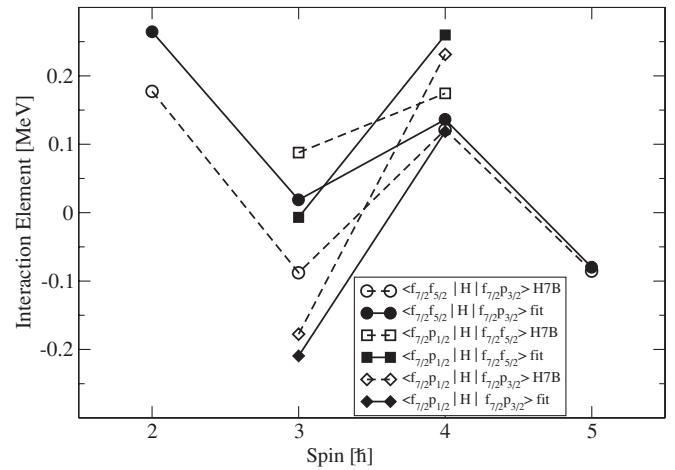FIG. 9. Same as Fig. 8, but for the $\pi f_{7/2}$ orbital.

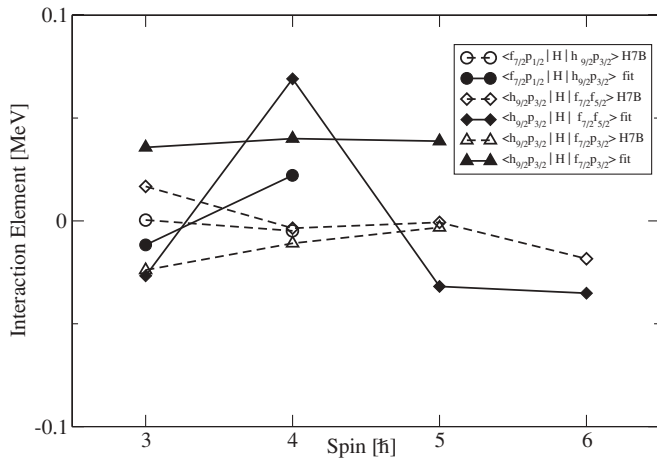FIG. 12. Nondiagonal interaction elements for the indicated configurations.

FIG. 10. Nondiagonal interaction elements for the indicated configurations.
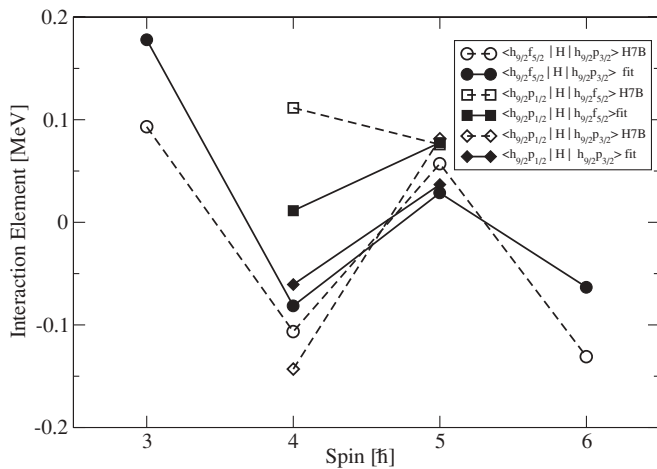

FIG. 11. Nondiagonal interaction elements for the indicated configurations.

of spins is very limited, to at most $4\hbar$, discerning a trend is difficult. Two cases show a pronounced odd-even staggering (not predicted by the H7B calculation), but for one case, the even spins are high, whereas the odd spin states are high for the other. For elements that involve the high lying $h_{9/2}f_{7/2}$ configuration, the agreement is worse (Table V), but they are also not so well determined from the experimental data.

Errors cannot be stated for the fitted nondiagonal elements; the correlations between the values for different elements are too strong to assign unique errors to individual elements. An overall estimate of the errors is, however, indicated as follows. The small differences between fitted and calculated elements change the γ-decay properties drastically. Therefore, in general, the differences between calculated and fitted values should be an upper limit for the errors. For very small elements, the error might accommodate a change in sign. It has been pointed out above, however, that the sensitivity of the data is vastly different for the various elements. The errors of the diagonal elements are small, estimated to be below 10 keV. The level energies are known to $\leqslant 1$ keV and resemble closely the matrix element of the dominant configuration, as admixtures of other configurations contribute only with the square of their amplitudes. These amplitudes are quite well determined and mostly small. But only the sums of the single-particle energies and the diagonal elements are really measured. Therefore the elements for all spins of a given configuration will shift by a common amount, if the single-particle energies are changed. The calculations of the interaction elements do not give any uncertainties either. Therefore it is not clear how good an agreement between experiment and theory might be expected.

IV. SUMMARY AND CONCLUSIONS

Conversion electrons have been measured for the decay of excited states in ^{208}Bi, populated in the ^{208}Pb(p, n) reaction, using both singles and coincidence techniques. The conversion coefficients extracted largely confirm the spin assignments for low- to medium-spin states, and electron-γ coincidences

have defined unambiguously decays to the 63 keV excited state. The measurements have confirmed the level scheme and multipolarity assignments from previous γ spectroscopy [1].

The firm assignments and relative completeness of the level scheme and the associated γ-ray transitions have allowed a detailed comparison with one-particle one-hole excitations in the context of the shell model.

The aim of testing the shell model was twofold. First, to address the adequacy of the model in terms of reproducing a broad range of experimental results, in this case, the measured energies, spectroscopic factors, electromagnetic decays, and γ-ray branching ratios, of states in ^{208}Bi, in detail and with empirical parameters. Second, to examine the matrix elements of the residual interaction that could be constrained experimentally, allowing a comparison with those calculated from the measured interaction between free nucleons.

In the calculations, the Kuo-Herling space of single-particle orbitals was used, meaning all orbitals between $83 \leqslant Z, N \leqslant 126$. Only one-particle one-hole states were considered with the implicit assumption that there is no mixing with two-particle two-hole and more complicated states. More precisely, small admixtures were treated by using effective operators. Thus, single-particle energies include contributions from the octupole excitation of the ^{208}Pb core, notably $i_{13/2}$ is mixed with $f_{7/2} \otimes 3^-$ and $f_{7/2}$ with $i_{13/2} \otimes 3^-$. The $M1$ and $E2$ matrix elements include the effects of magnetic and quadrupole core polarization. Most of these parameters have been taken from experiment and include therefore these, and possibly other effects, automatically. These effects of core excitations are specific for ^{208}Pb and their influence might change for nuclei more remote from this core.

The matrix elements of the residual interaction were fitted by a least-squares procedure to the experimental data. As an intermediate step, diagonalization of the Hamiltonian gave the wave functions from which energies and spectroscopic factors follow directly. $M1$ and $E2$ γ-decay strengths were calculated by angular momentum coupling from the single-particle elements. Fitting of the interaction elements rather than the wave functions as an initial step has the advantage

that the symmetry condition of the Hamiltonian simplifies the fit, while the equivalent orthonormality requirement for the wave functions would otherwise pose a major complication. Energies and spectroscopic factors were easily reproduced, but also nearly all measured γ-branching ratios were successfully reproduced, despite their sensitivity to small admixtures of the wave functions and therefore the mixing matrix elements. In conclusion, the shell model with the specified restrictions was able to give the wave functions in sufficient detail to reproduce a range of very sensitive γ-decay properties.

In the process, 150 elements of the residual interaction have been fitted. About 100 of these that involve only lower lying configurations are very reliably determined, as there is an abundance of data and the results depend very little on the less well-known properties of high lying states. The uncertainty of the matrix elements increases when proceeding to energetically higher configurations. This extensive set of experimental interaction elements, including nondiagonal ones, is new and can be used to test calculations of the interaction. It might be noted that nondiagonal elements are unambiguously determined and therefore more meaningful. Diagonal elements in contrast depend on the choice of single-particle energies as only their sum can be measured. It might be noted that experimental single-particle energies have been used that are influenced by core excitations. The agreement with the realistic interaction derived from the H7B parametrization is, overall, very good. The comparison may also be useful in showing how to improve the calculations, and the results could be valuable for recent calculations with low momentum interactions [3] that can be applied to a much wider range of nuclei.

[1] P. Boutachkov, K. H. Maier, A. Aprahamian, G. V. Rogachev, L. O. Lamm, M. Quinn, B. B. Skorodumov, and A. Woehr, Nucl. Phys. **A768**, 22 (2006).

[2] T. T. S. Kuo and G. E. Brown, Nucl. Phys. **85**, 40 (1966).

[3] S. Bogner, T. T. S. Kuo, L. Coraggio, A. Covello, and N. Itaco, Phys. Rev. C **65**, 051301(R) (2002).

[4] M. P. Kartamyshev, T. Engeland, M. Hjorth-Jensen, and E. Osnes, Phys. Rev. C **76**, 024313 (2007).

[5] W. P. Alford, J. P. Schiffer, and J. J. Schwartz, Phys. Rev. C **3**, 860 (1971).

[6] G. M. Crawley, E. Kashy, W. Lanford, and H. G. Blosser, Phys. Rev. C **8**, 2477 (1973).

[7] M. J. Martin, Nucl. Data Sheets **47**, 797 (1986).

[8] M. Guttormsen, H. Huebel, A. v. Grumbkow, Y. K. Agarwal, J. Recht, K. H. Maier, H. Kluge, A. Maj, M. Menningen, and N. Roy, Nucl. Instrum. Methods A **227**, 489 (1984).

[9] T. Kibédi, G. D. Dracoulis, and A. P. Byrne, Nucl. Instrum. Methods A **294**, 523 (1990).

[10] T. Kibédi, G. D. Dracoulis, and A. P. Byrne, Research School of Physical Sciences and Engineering, Australian National University, Dept. of Nuclear Physics, Annual Report 2001, p. 128, and earlier annual reports.

[11] P. A. Butler, P. M. Jones, K. J. Cann, J. F. C. Cocks, G. D. Jones, R. Julin, and W. H. Trzaska, Nucl. Instrum. Methods A **381**, 433 (1996).

[12] T. Kibédi, T. W. Burrows, M. B. Trzhaskovskaya, and C. W. Nestor, AIP Conf. Proc. **769**, 268 (2005).

[13] B. Fornal, R. Broda, K. H. Maier, P. J. Daly, P. Bhattacharyya, Z. W. Grabowski, W. Krolas, T. Pawlat, J. Wrzesinski, M. P. Carpenter *et al.*, Phys. Rev. C **67**, 034318 (2003).

[14] M. Rejmund, M. Schramm, and K. H. Maier, Phys. Rev. C **59**, 2520 (1999).

[15] P. Ring, R. Bauer, and J. Speth, Nucl. Phys. **A206**, 97 (1973).

[16] R. Bauer, J. Speth, V. Klemt, P. Ring, E. Werner, and T. Yamazaki, Nucl. Phys. **A209**, 535 (1973).

[17] B. Fornal, R. Broda, K. H. Maier, J. Wrzesinski, G. J. Lane, M. Cromaz, A. O. Macchiavelli, R. M. Clark, K. Vetter, A. P. Byrne *et al.*, Phys. Rev. Lett. **87**, 212501 (2001).

[18] M. Anselment, W. Faubel, S. Goering, A. Hanser, G. Meisel, H. Rebel, and G. Schatz, Nucl. Phys. **A451**, 471 (1986).

[19] K. H. Maier, T. Nail, R. K. Sheline, W. Stoeffl, J. A. Becker, J. B. Carlson, R. G. Lanier, L. G. Mann, G. L. Struble, J. A. Cizewski *et al.*, Phys. Rev. C **27**, 1431 (1983).

[20] A. Hosaka, K. I. Kubo, and H. Toki, Nucl. Phys. **A444**, 76 (1985).

[21] S. P. Pandya, Phys. Rev. **103**, 956 (1956).

[22] K. H. Maier and M. Rejmund, Eur. Phys. J. A **14**, 349 (2002).

[23] J. P. Schiffer and W. W. True, Rev. Mod. Phys. **48**, 191 (1976).